

AD-A034 900

AIR FORCE INST OF TECH WRIGHT-PATTERSON AFB OHIO SCH--ETC F/6 20/5
EFFECTS OF OXYGEN CONTAMINANT CN ON GAS DYNAMIC LASER PERFORMANC--ETC(U)
DEC 76 J B WATTERSON

UNCLASSIFIED

6EP/PH/76D-12

NL

1 of 2

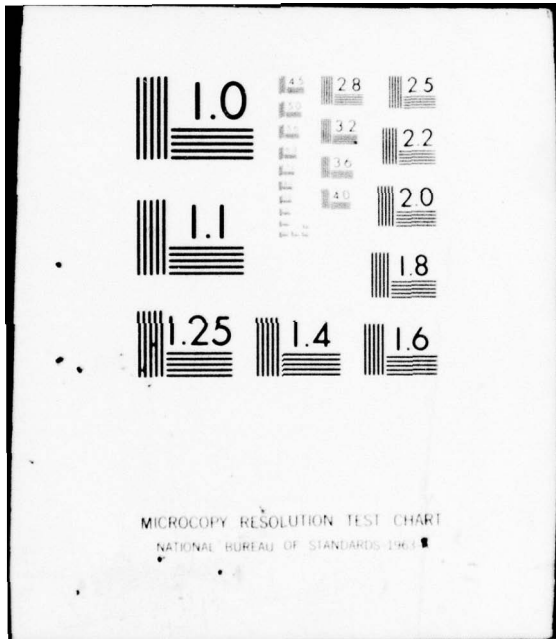
AD
AO34900



This block contains a grid of 120 small document pages, arranged in 10 rows and 12 columns. Each page is a miniature version of a technical document, likely a slide or a page from a report. The pages contain various types of content, including:

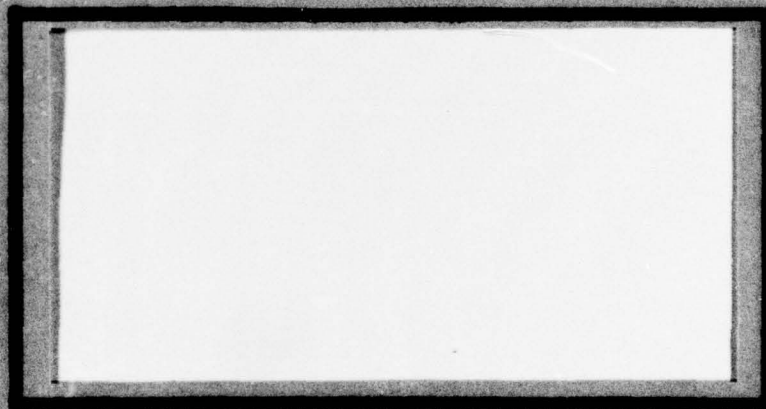
- Textual paragraphs and sections.
- Diagrams and flowcharts.
- Tables and data charts.
- Graphs and plots.
- Equations and mathematical expressions.

The pages are densely packed and cover most of the lower two-thirds of the document's page area.



MICROCOPY RESOLUTION TEST CHART
NATIONAL BUREAU OF STANDARDS-1963-A

ADA 034900



J
D D C
RECEIVED
JAN 27 1971
C

UNITED STATES AIR FORCE
AIR UNIVERSITY
AIR FORCE INSTITUTE OF TECHNOLOGY
Wright-Patterson Air Force Base, Ohio

DISTRIBUTION STATEMENT A
Approved for public release
Distribution Unlimited

D D C
D D C
JAN 27 1977
D D C

⑥ EFFECTS OF OXYGEN CONTAMINATION
ON GAS DYNAMIC LASER PERFORMANCE

⑨ Master's THESIS,

⑭ GEP/PH/76D-12

⑩ John B. Watterson
Capt USAF

⑪ Dec 76

⑫ 117p.

012 225
log

EFFECTS OF OXYGEN CONTAMINATION
ON GAS DYNAMIC LASER PERFORMANCE

THESIS

Presented to the Faculty of the School of Engineering
of the Air Force Institute of Technology

Air University

in Partial Fulfillment of the
Requirements for the Degree of

Master of Science

by

John B. Watterson, B.S.

Capt USAF

Graduate Engineering Physics

December 1976

NTIS	White Section	<input checked="" type="checkbox"/>
DTIC	Off Section	<input type="checkbox"/>
IDENTIFICATION		
BY DISTRIBUTION/AVAILABILITY CODE		
Yes	NO	SPECIAL
A		

Table of Contents

Preface	iii
List of Figures.....	v
List of Tables.....	vii
List of Symbols.....	viii
Abstract.....	x
I. Introduction.....	1
Gas Dynamic Laser Basics	1
Previous Studies.....	5
Purpose	7
II. Historical Development.....	9
Early Laser Development.....	9
Gas Dynamic Laser Development.....	10
III. Theory.....	14
Processes in the GDL.....	14
Four-Temperature Kinetics Code.....	17
J-Line Scan Analysis.....	20
IV. Experimental Apparatus and Procedure.....	24
Shock Tube Facility.....	24
Gas Manifold Assembly.....	30
Air Table Apparatus.....	34
V. Results and Discussion.....	42
Presentation of Data.....	42
Results.....	43
Discussion.....	50
VI. Suggestions and Recommendations.....	69
Bibliography.....	71
Appendix A: Raw Gain Data.....	73
Appendix B: Fabrication Drawings.....	79
Appendix C: List of Equipment.....	82
Appendix D: Data on Instruments.....	84
Appendix E: Area Ratio Data.....	86

Table of Contents (cont)

Appendix F: Derivation of Small-Signal Gain.....	86
Appendix G: Derivation of Energy Available for Lasing.....	89
Vita.....	92

Preface

This thesis is a summary of my research efforts over the past few months on the effect of oxygen contamination in the fuel mixture of a shock-tube driven gas dynamic laser. This project constitutes one segment of continuing studies being conducted at the Advanced Radiation Technology Office (ARTO) located at Kirtland AFB, New Mexico. I feel privileged to have been able to conduct this experiment; not only was this study new and unique, but also the project was extremely rewarding. By performing this experiment, I believe I learned of gas dynamic lasers, their operation and their performance, and about experimental technique and conduct. In spite of all the minor setbacks and equipment failures that seem to hamper every experiment, the experience I gained far out-balances the frustrations I encountered. It has been said that in an experimental science, truth is always an observation. Thus, it is a most profound reward indeed to conduct a series of tests that yield those observations.

The successful operation of a project such as this thesis necessitates contributions from many people of various specialties. My gratitude is extended to Colonel D. H. Lambertson, Commander of ARTO, who sponsored my activities during this summer. I wish to thank Dr. Steven G. Hadley, Chief of the Gas Dynamic Laser Section at ARTO, for his help and assistance during this experiment. I am especially indebted to Captain Allen M. Hunter, II, of the Air Force Institute of Technology. Through his patience and understanding Captain Hunter helped

guide me along the numerous paths traversing the forest of gas dynamic laser technology. It is to Al that I owe my deepest thanks. Finally, I would like to express a special debt of gratitude to three of my companions of this summer, Dr. G. Stuart Knoke, Master Sergeant Rudolph Vargas, and Mr. Frank P. Wingate. Without the help that they gave so willingly and the experience they imparted so freely, this project would not have been successful. I am pleased to not only know Stu, Frank and Rudy as my tutors, but also as my friends.

List of Figures

<u>Figure</u>		<u>Page</u>
1	Schematic of Major Gas Dynamic Laser Components	2
2	General Conditions for a Gas Dynamic Laser	4
3	Previous Studies of Excess Oxygen Contamination	6
4	Peak Gain as a Function of H ₂ O Content for First- and Second-Generation GDLs	13
5	Fundamental Modes of Species in a GDL	16
6	Variation in Temperatures with Distance from Nozzle Throat for Three Gas Compositions	19
7	Shock Tube Conditions	25
8	Pressure Histories in a Shock Tube	27
9	Pressure Thresholds for Diaphragms	28
10	Shock Tube Gas Manifold Assembly	32
11	Schematic of Experimental Apparatus	37
12	Photographs of Experimental Apparatus	39
13	Oscillogram from which Gain Measurement is Made	41
14	J-Line Scan: 0% O ₂ Case	45
15	J-Line Scan: 10% O ₂ Case	48
16	J-Line Scan: 20% O ₂ Case	52
17	J-Line Scan: 30% O ₂ Case	55
18	J-Line Scan: 40% O ₂ Case	58
19	T, T ₁ versus Percent Oxygen	60

List Of Figures (Cont)

<u>Figure</u>		<u>Page</u>
20	T_N, T_3 versus Percent Oxygen	62
21	Interpolated Peak Gain versus Percent Oxygen	64
22	Energy Available versus Percent Oxygen	66

List of Tables

<u>Table</u>		<u>Page</u>
I	Experimental Results 0% Oxygen Contamination	44
II	Interpolated Results 0% Oxygen Contamination	46
III	Experimental Results 10% Oxygen Contamination	47
IV	Interpolated Results 10% Oxygen Contamination	49
V	Experimental Results 20% Oxygen Contamination	51
VI	Interpolated Results 20% Oxygen Contamination	53
VII	Experimental Results 30% Oxygen Contamination	54
VIII	Interpolated Results 30% Oxygen Contamination	56
IX	Experimental Results 40% Oxygen Contamination	57
X	Interpolated Results 40% Oxygen Contamination	59

List of Symbols

A/A^*	Nozzle Area Ratio
$CO_2^*(\nu_1)$	Symmetric stretch (100) mode
$CO_2^*(\nu_2)$	Bending (010) mode
$CO_2^*(\nu_3)$	Asymmetric Stretch (001) mode
E_A	Energy Available for Lasing
$F(m)$	Function for the variation of the vibrational transition matrix element with rotational transition (Ref 18) $= 1 - 0.0009m - 0.00006m^2$
g	Small-signal gain coefficient (cm^{-1})
h^*	Nozzle throat height
J_u	Rotational quantum number of upper laser level
J_l	Rotational quantum number of lower laser level
m	$= -J_l = -(J_u + 1)$ for P-branch transitions
N_c	Number density of CO_2 molecules
Q_r^{-1}	Rotational partition function $= 2\theta_r/T$
Q_v^{-1}	Vibrational partition function $= (1 - \exp(-1920/T_1)) (1 - \exp(-960/T_1))^2 (1 - \exp(-3380/T_3))$
T	Gas Temperature
S_J	A convenience factor $= \lambda_m/\lambda_o F(m) m $
R^2	Vibrational transition Matrix element $= 1.61 \times 10^{-39}$ erg-cc for CO_2 (100-001) (Ref 18)
R_u	Universal Gas Constant
T_1	Vibrational temperature of CO_2 (100)
T_2	Vibrational temperature of CO_2 (020)
T_3	Vibrational temperature of CO_2 (001)
T_l	Vibrational Temperature of lower laser level

List of Symbols (Cont)

ϕ	Line shape factor
λ_m	Wavelength of a particular vibraional-rotational transition
λ_0	Reference wavelength = 10.42 microns
v_i	Mole fraction of I-th species
θ_r	Rotational constant, $\text{CO}_2 = .56^\circ\text{K}$
θ_1	Characteristic temperature of CO_2 (100)
θ_2	Characteristic temperature of CO_2 (020)
θ_3	Characteristic temperature of CO_2 (001)
θ_l	Characteristic temperature of lower laser level
σ_i	Optical broadening cross-section for CO_2 colliding with the i-th species

Abstract

The effects of oxygen contamination in the fuel mixture of a shock-tube driven gas dynamic laser was observed using the four-inch shock tube of the Air Force Weapons Laboratory (AFWL) at Kirtland AFB, New Mexico. Five test gases comprised of CO_2 , N_2 , O_2 , and H_2O were studied; the mixtures varied in that O_2 was allowed to replace the N_2 content. Oxygen replaced nitrogen in the mixtures in 10% increments, starting from a baseline case of 10% CO_2 , 87% N_2 , and 3% H_2O to a mixture containing 40% O_2 , 10% CO_2 , 47% N_2 , and 3% H_2O .

The small-signal gain coefficient was measured on three different rotational transitions, allowing a J-line scan to be made for each test gas. The gain coefficient, g , was found to decrease linearly as the O_2 content increased. It was also observed that an increase in the O_2 content of one percent resulted in a degradation of g by 1.5%. The observed decrease in g is in agreement with previous work performed at AFWL.

Energy available for lasing, E_A , was investigated using a J-line scan technique. It was found that E_A experienced a linear decrease as O_2 was introduced into the test gas. The value for E_A of the baseline mixture was interpolated to be 15.3 ± 4 KJ/lb, while that of the gas mixture containing 40% excess oxygen was 5.9 ± 4 KJ/lb.

EFFECTS OF OXYGEN CONTAMINATION
ON GAS DYNAMIC LASER PERFORMANCE

I. Introduction

Gas Dynamic Laser Basics

Since its inception more than 10 years ago, the gas dynamic laser (GDL) has been in the forefront of high-energy laser devices. GDLs use rapid fluid dynamic expansions to create population inversions in the vibrational energy distributions of certain molecules in the lasing medium. The major components of a gas dynamic laser are shown in Figure 1. Combinations of gases, typically CO_2 , N_2 , and He or H_2O are heated in the combustion chamber to a stagnation temperature of about 2000 degrees Kelvin and to a pressure of about 300 psi. This hot, high-pressure gas mixture is then expanded through the second major GDL component, the nozzle array.

As the gas flows through this array of nozzles, typically at flow speeds of Mach four, it is expanded and cooled. This rapid, adiabatic expansion reduces the translational and rotational energies of the molecules in the mixture. Because the vibrational relaxation time is long compared to the expansion time, the expansion process produces a population inversion in some of the vibrational energy levels of the gas. That is, the energy (characterized by a temperature) of molecules in the symmetric stretch (100) vibrational mode of CO_2 becomes roughly equilibrated with the gas translational temperature. Although the (100) mode temperature approaches the

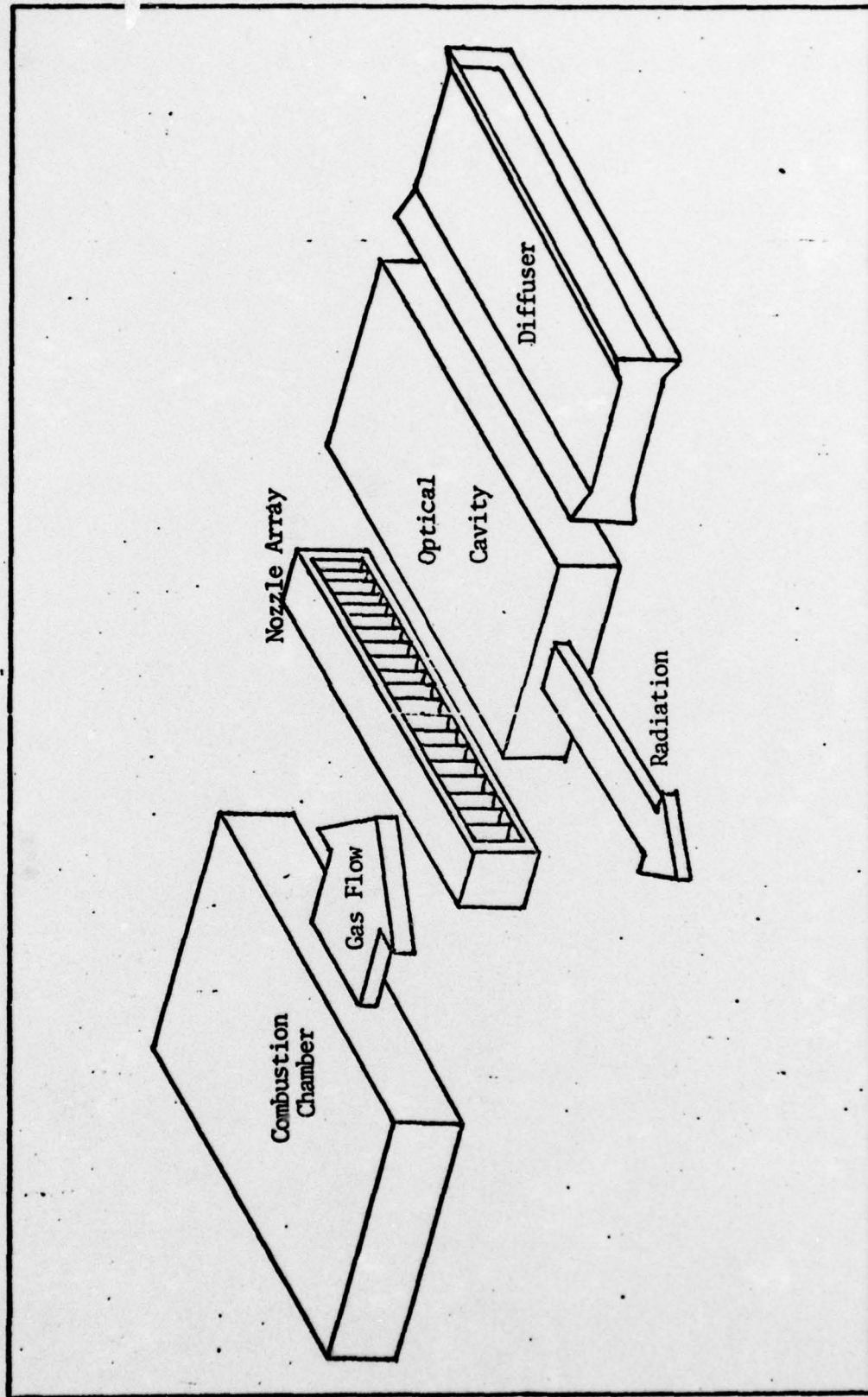


Fig. 1. Schematic of Major Gas Dynamic Laser Components.

gas temperature, the energy (hence temperature) of the asymmetric stretch (001) remains near the reservoir or stagnation temperature. The population of the energy levels, which previously followed a Boltzmann distribution in the stagnation region, is inverted in the laser cavity. There are now more CO_2 molecules in the (001) mode than in the (100) mode and lasing can now be achieved. A graphic description of this process is shown in Figure 2.

Figure 2A shows a typical set of GDL nozzles; to the left of the nozzles lies the stagnation region, to the right lies the optical cavity. Figure 2B depicts how the energy is distributed in a GDL. Finally, Figure 2C schematically portrays the populations of CO_2 molecules in the (100), lower laser level, mode and in the (001), upper laser level, mode. Here N_x refers to the number of molecules in excited mode and N_{000} is the number of CO_2 molecules in the ground state.

After the population inversion has been achieved, the gas flows into the third GDL component, the laser cavity. Located immediately downstream of the nozzle array, optical energy can be extracted perpendicular to the flow in this region. As Figure 1 shows, the mixture is then channeled into the fourth major component of the GDL, the diffuser, which slows the gas to subsonic speeds and raises the pressure of the gas. The mixture is then exhausted, generally to the atmosphere.

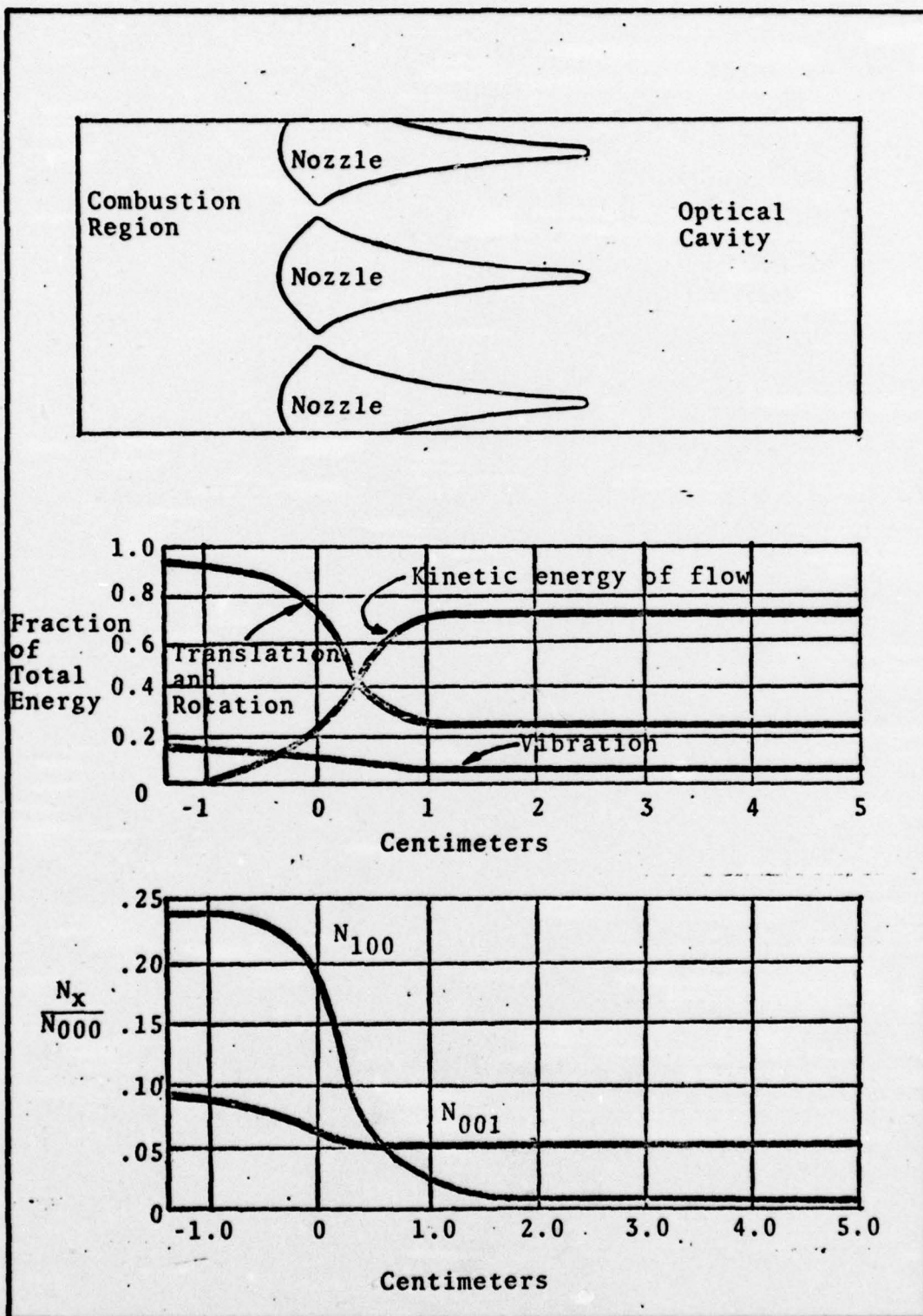


Fig. 2. General Conditions for a Gas Dynamic Laser (Ref 1:54)

Previous Work

The effects of O_2 in the fuel (i.e. excess O_2) of GDLs has been previously studied (Refs 2, 3). However, discrepancies between the two published reports on oxygen contamination do exist. As pointed out in Reference 3, an examination of the data presented in Reference 2 reveals a possible inconsistency. Figure 3A shows a replot of the data of Reference 2; gain versus percent excess O_2 (including the baseline case of zero percent O_2) is shown. It is evident that there is a distinct trend in the gain curve of the mixtures containing excess oxygen. As can be seen from Figure 3A, for mixtures with greater than five percent O_2 , each additional percent of O_2 reduces the gain by about one percent (Ref 3:134). However, Figure 3A also reveals that the gain drops off dramatically for the baseline case. On the other hand, as shown in Figure 3B, the data of Reference 3 contradicts this decrease in gain in mixtures containing between zero and five percent excess O_2 . Instead, Reference 3 indicates that the gain degradation is proportional to the amount of excess O_2 in the fuel mixture, starting from the baseline case. The gain data shown in Figure 3B are interpolated values of the peak, $P(20)$, gain; coefficient measurements were taken about seven cm downstream of the nozzle throat. Figure 3B shows that, starting from the baseline case, each percent of O_2 results in roughly a 1.1% loss in gain.

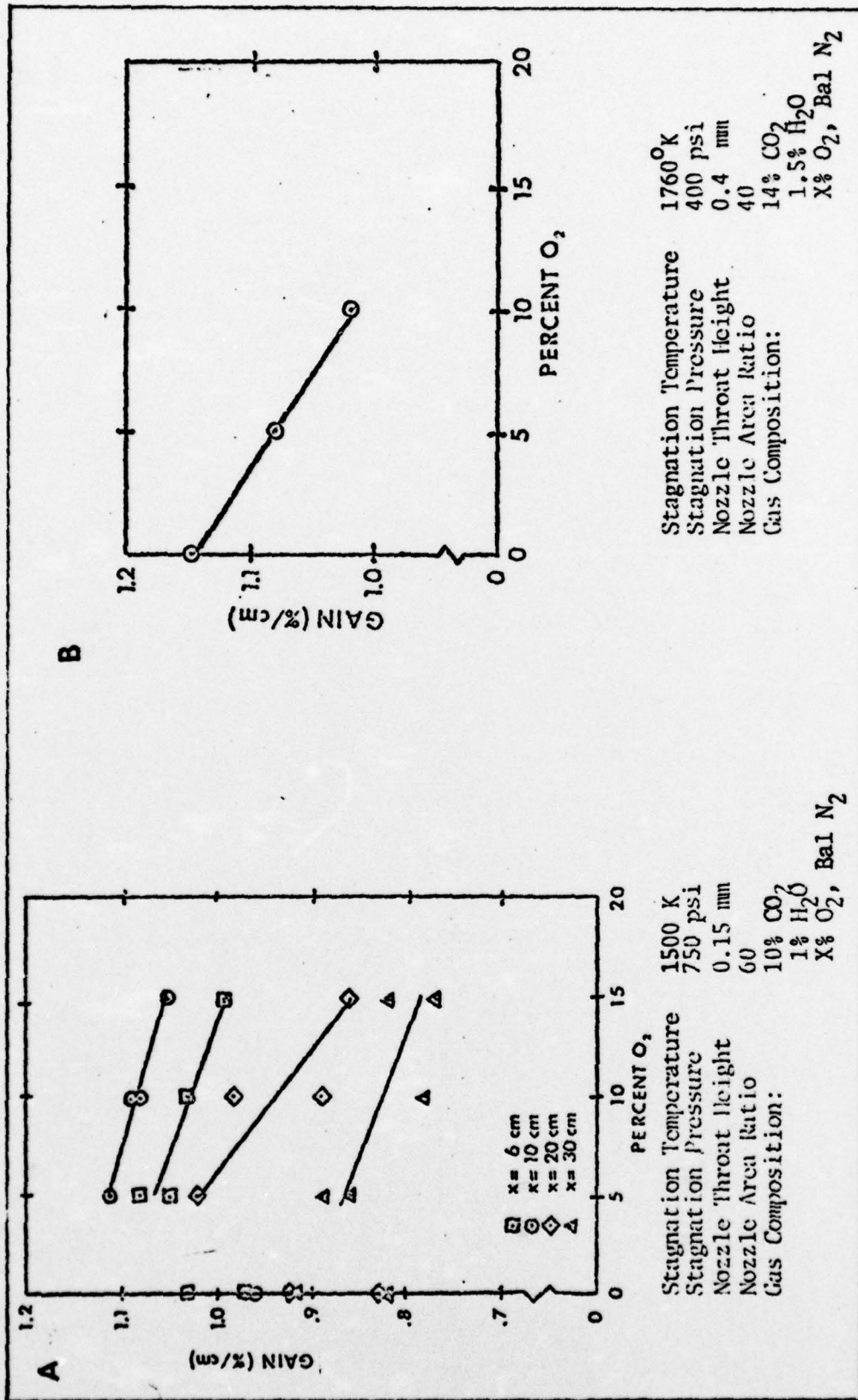


Fig. 3. Previous Studies of Excess Oxygen Contamination (Ref 3).

The Present Study

The purpose of this study is to investigate effects due to the presence of oxygen in the fuel mixture of a shock-tube driven gas dynamic laser. This study, undertaken at the United States Air Force Weapons Laboratory, Kirtland AFB, New Mexico, was performed in the Summer of 1976. The experiment involved the addition of oxygen, in 10-percent mole fraction increments, to an arbitrary GDL fuel mixture of 10 percent CO_2 and 3 percent H_2O , with the balance being made up by N_2 . The amount of oxygen that replaced nitrogen in the fuel mixture ranged from 0% (the baseline case) to 40%; thus, the fuel mixture at maximum O_2 content consisted of 10% CO_2 , 3% H_2O , 47% N_2 , and 40% O_2 .

The small-signal gain coefficient at line center, designated by the letter "g", was measured twelve times for each of the five gas compositions. As will be shown later, the measurement of gain on different rotational lines of CO_2 can be used to calculate not only the translational temperature of the GDL fuel, but also to find a value for the maximum energy available for lasing. The energy available for lasing is an important parameter for the gas dynamic laser, and will be designated " E_A " in this report. The method used to calculate the gas temperature and E_A is based on an experimental technique known as a J-line scan. In this procedure, the gain coefficient, g, was measured on a variety of J (rotational) lines of CO_2 , the lasing molecule. In this experiment, g was measured four times on each of three

different P-branch transitions for each gas composition. The transitions on which the gain was measured were arbitrarily chosen to be the P-12, P-30, and either the P-20 or P-18 lines. The results of the J-line scan are presented later in this study.

As will be discussed on page 11 of this report, the presence of oxygen in the fuel of gas dynamic lasers is an undesirable but necessary facet of state-of-the-art GDLs. The compounds which fuel these third-generation devices normally produce oxygen which amounts to 20 to 25 percent of the total fuel composition. Additionally, those compounds also tend to produce H_2O in the fuel which ranges from three to eight percent of the composition. These 'contaminating' species of O_2 and H_2O in the fuel of GDLs force the laser well away from its optimum performance capabilities. This study was necessary to verify O_2 contamination in the fuel mixture of a GDL results in a predictable degradation in performance.

Organization

The following paper will be divided into five sections. First, a brief historical development of the gas dynamic laser will be given. A survey of basic GDL theory as well as a description of the AFWL GDL four-temperature model and J-line scan technique will be presented next. Chapter Four will be devoted to a description of the experimental approach. Reduced data will be presented in Chapter Five. Finally, suggestions and recommendations for follow-on experiments will be presented.

II. Historical Development

Early Laser Development

The history of the gas dynamic laser can be traced back to the early 1960's. In this time frame, T. H. Maiman of Hughes Research Laboratories demonstrated lasing action from chromium-doped ruby crystal (Ref 4:493). The first gas laser closely followed Maiman's ruby laser. In 1961, A. Javan, et al, of Bell Laboratories initiated the first gas laser, which operated on a transition between two excited states of Ne (Ref 5:106). This laser development led to increased interest in methods of obtaining population inversions in gases other than Ne. As early as 1962, Abraham Herzberg and his colleagues at the Cornell Aeronautical Laboratory suggested that a rapid expansion in a gas could produce a population inversion (Ref 6:1). Also at this same time, Soviet scientists, Basov and Oraevskii, showed that a rapid gas dynamic expansion could produce the nonequilibrium required for a population inversion (Ref 7:1742). The development of the CO₂ gas laser by C.K.N. Patel at the Bell Telephone Laboratories (Ref 6:5) brought forth a very good lasing medium for the still theoretical GDL system. A theoretical analysis by N. Basov, et al, then showed that the CO₂-N₂ medium, upon rapid expansion in a laval-type nozzle, did indeed constitute a feasible laser scheme (Ref 6:5). The first practical demonstration of a GDL was carried out by the AVCO Everett Research Laboratory in the fall of 1970 (Ref 1:54). Powered by what was essentially a small rocket, this first model pro-

duced 6,000 W of power for 10 seconds. Further, the cross-sectional area of the optical cavity was only 3 by 30 cm. Thus, within ten years of its origin, the laser had evolved to a high-energy device in the form of a GDL that produced thousands of watts power for relatively long periods of time. The GDL was now at the forefront of high-energy laser technology.

Gas Dynamic Laser Development

Gas dynamic lasers have undergone three fundamental design changes (Ref 8:89). The first-generation GDLs, initiated by the AVCO invention discussed above, are characterized by stagnation temperatures and pressures of approximately 1000 to 1500 degrees K and 14 to 25 atm. The ratio of the nozzle exit area to the nozzle throat area (A/A^*) on these devices is typically around 20, and the nozzle throat height (h^*) is about 1 mm. For example, the first AVCO model operated at 1300 °K and 17 atm. The A/A^* value of this laser was 14, and $h^* = 0.8$ mm. The fuel mixture on this device was 8% CO_2 , 0.2% CO , 91% N_2 , and 0.8% H_2O . Second-generation GDLs exhibit higher stagnation conditions (roughly 1500 to 2000 °K and 30-50 atm). Additionally, they operate with larger area ratios (on the order of 50) and smaller throat heights (typically 0.2 to 0.3 mm). The basic fuel mixture of the second-generation GDLs remains approximately the same as that used by their predecessors, with one important exception: the second-generation fuel mixture contains a greater percentage of H_2O , about

three percent of the total fuel (Ref 8:89). The third generation GDL is the newest gas dynamic laser variant to be presented. Typical stagnation temperatures for this class of GDLs are between 2000 and 2500 degrees K, with accompanying stagnation pressures in excess of 100 atms (Ref 8:107). The area ratio of this newest GDL has been enlarged to 100 and the nozzle throat height has decreased to about 0.1 mm (Ref 9). Perhaps the most significant facet of the third-generation GDLs is that these devices are fueled with bireactant compounds. That is, instead of a combination of gases such as CO_2 , N_2 , H_2 , and O_2 , these bireactant gas dynamic lasers (BRGDLs) use two compounds which react to form a quantity of gas that has potential for lasing. Unfortunately, whereas in the first- and second-generation gas dynamic laser the fuel mixture could be adjusted to contain just the correct amounts of CO_2 , N_2 , and H_2O , the bireactant character of the third-generation GDL does not lend itself to the optimization of the gas mixtures. For example, the reaction of one fuel-oxidizer candidate (JP-4 and N_2O) produces O_2 in excess of 25 to 30 percent (Ref 9). Additionally, bireactant compounds produce H_2O in amounts that decrease gain and energy available for lasing, E_A . For example, the BRGDL at the Weapons Laboratory operates on a fuel-oxidizer mixture that typically yields 20% excess O_2 and 4 to 8% excess H_2O . The excessive oxygen content pushes the operation of the BRGDL well away from optimum values of E_A as well as gain. Additionally, the amount of water present in the mixture prohibits optimum gain and E_A values

from being attained. The effect of contaminants, specifically excess H_2O , on gain for first- and second-generation GDLs has been previously studied (Ref 10:32). Figure 4 shows how H_2O affects the gain in such devices. As shown in the figure, peak gain in first-generation GDLs is degraded by H_2O in amounts over about two percent. Second-generation GDLs tolerate up to three percent H_2O before the gain is decreased. No experimental evidence is available for optimum H_2O content in BRGDLs, but it is considered that H_2O in amounts of seven to eight percent are indeed excessive for third-generation devices (Ref 9).

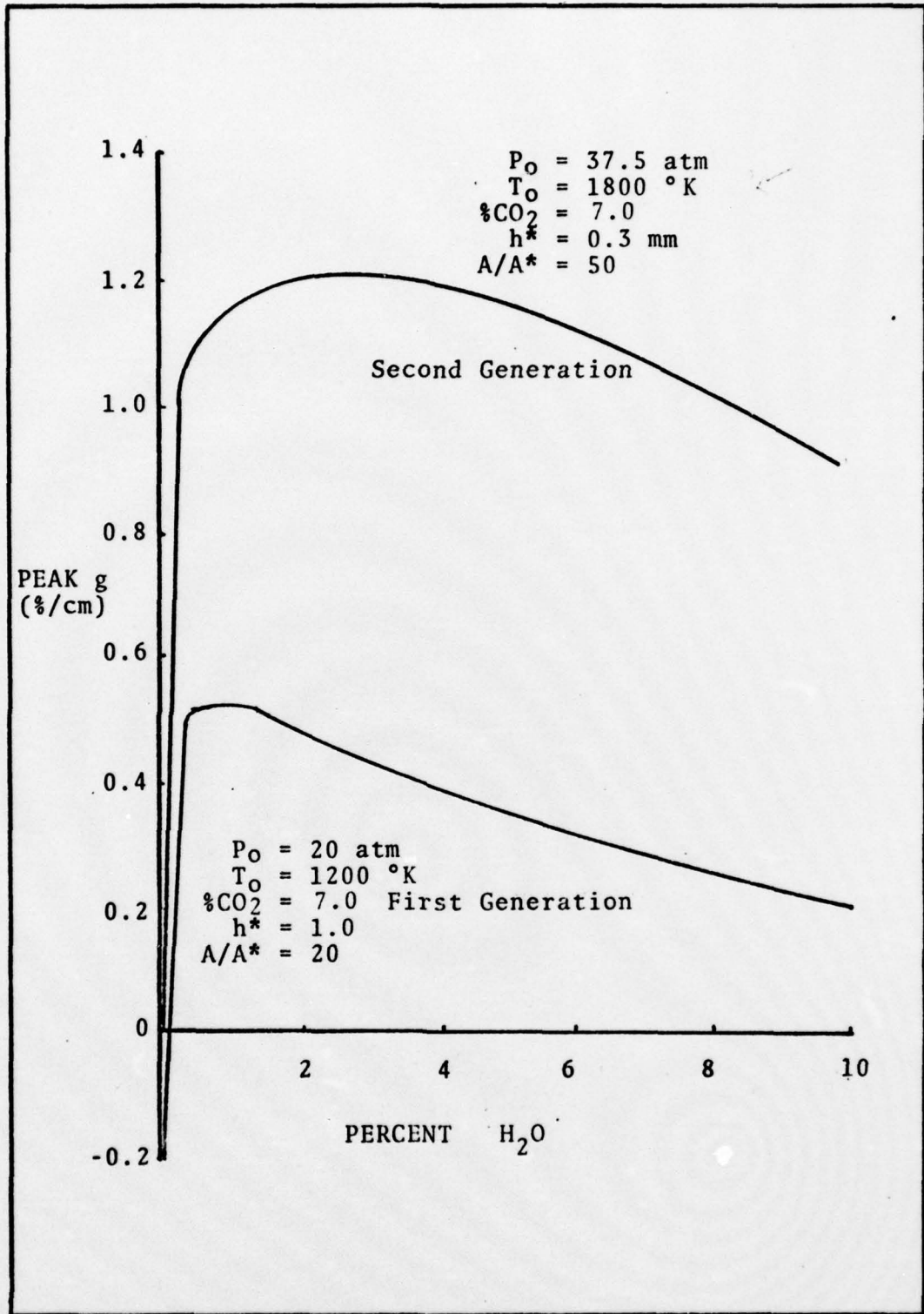
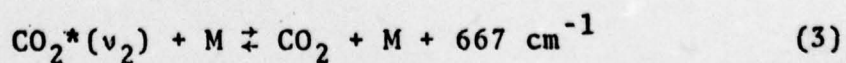
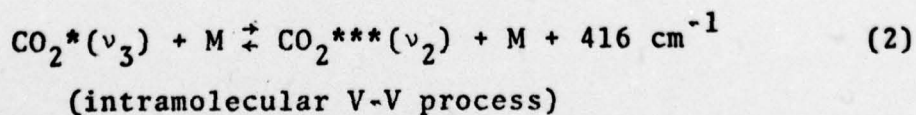
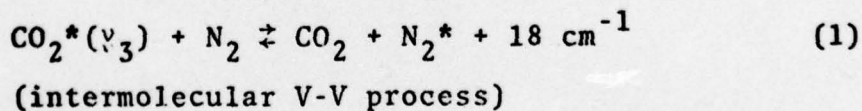
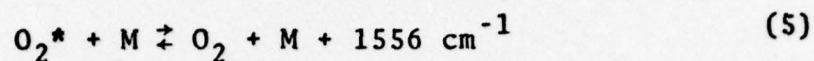
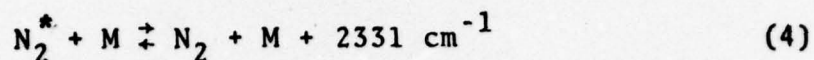


Fig. 4. Peak Gain as a Function of H_2O Content for First- and Second-Generation GDLs (Ref 11:32).

III. TheoryProcesses in the GDL

The laser mixture used in this experiment generally contained CO_2 , H_2 , H_2O , and O_2 . CO_2 is the active lasing molecule, N_2 stores vibrational energy and pumps the upper laser level, and H_2O (in the correct amount) preferentially relaxes the lower laser level. Oxygen acts as an inert substance in the laser, and in this experiment, O_2 replaced and diluted the nitrogen content of the mixture. The CO_2 - N_2 - H_2O - O_2 molecules are regularly colliding with each other in the lasing medium. Several different energy transfer processes occur between the various modes of CO_2 and other molecules. Using the notation of Reference 11, the important levels are the excited nitrogen levels, N_2^* , the upper laser level $\text{CO}_2^*(\nu_3)$, and the lower laser level $\text{CO}_2^*(\nu_1)$. It is assumed that the bending mode, $\text{CO}_2^{**}(\nu_2)$, and the lower laser level are in thermal equilibrium due to Fermi resonance (Ref 12:2612). The important kinetic reactions involving the laser medium in the GDL are (Ref 11:27):





(V-T Processes)

In the above equations M stands for a collision partner that can be CO_2 , N_2 , H_2O , or O_2 . The asterisks indicate the vibrational level of a species in a given mode. Figure 5 shows the vibrational energy diagram for the CO_2 - N_2 - H_2O - O_2 system. Each of the vibrational modes can be assigned its own characteristic temperature. Because of the Fermi resonance existing between the (100) and (020) vibrational modes of CO_2 , both can be assumed to have the same temperature. The combined temperature is T_ρ , the lower laser level temperature. The vibrational temperature of the (001) mode of CO_2 is T_3 , and T_N is the temperature of $N_2(V=1)$ vibration. With the translational-rotational temperature, T, there are four distinct temperatures describing the vibration system (Ref 13:92).

Water serves to deactivate the lower laser level through T-V process described by Eq (3). At 400 °K, the rate of deactivation of the bending mode of CO_2 by H_2O is about three orders of magnitude higher than the rates of deactivation by O_2 , N_2 or CO_2 (Ref 14:4). Water (in correct proportions) therefore deactivates the bending mode of CO_2 rather well, while the presence of O_2 has little effect on the relaxation of $CO_2^*(v_2)$. For this reason, oxygen contamination is considered to have little effect in the fuel mixture of a GDL except as a diluent (Refs 2:64, 10).

However, the V-T deactivation of O_2^* (described by Eq

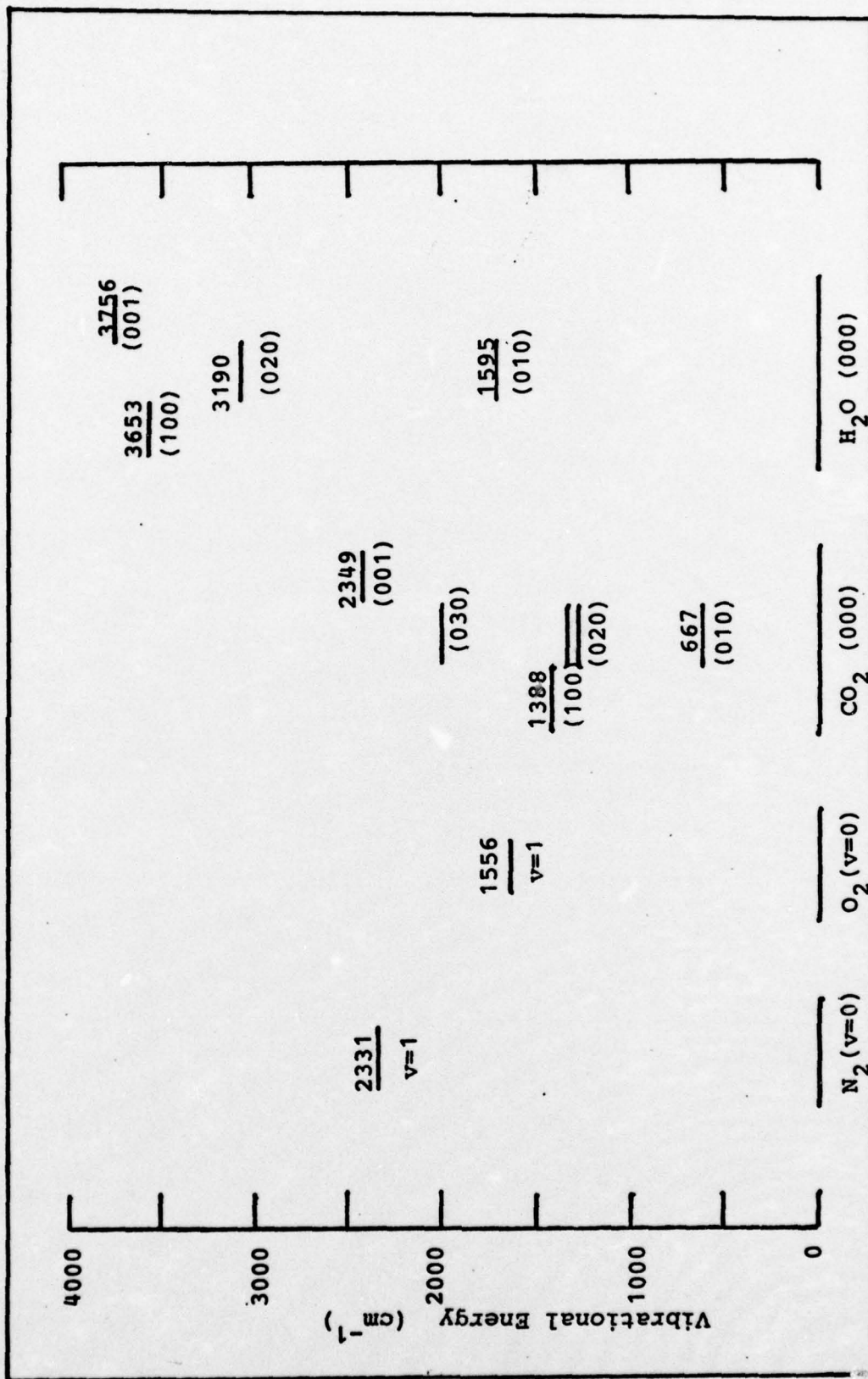


Fig 5. Fundamental Modes of Species in a GDL (Ref 14).

(5) is important. Water preferentially deactivates excited O_2 ; the rate of deactivation by H_2O on this mode is four orders of magnitude higher than the rate by other species such as N_2 or O_2 (Ref 14:6). The deactivation of O_2 by H_2O is an exothermic process, and this adds heat to the fuel mixture.

The replacement of N_2 by O_2 reduces the population of the pumping species in the vibrational system. Because there are fewer N_2 molecules to pump the CO_2 molecules, the population of the upper laser level is decreased. The decline in $CO_2^*(v_3)$ molecules, while still enough for a population inversion, degrades the small-signal gain coefficient and brings about a loss in energy available for lasing. Because O_2^* is deactivated readily by H_2O , the temperature of the gas rises with increasing O_2 content. As N_2 is replaced in the mixture, the upper laser level equilibrates more quickly with the gas temperature.

Four-Temperature Kinetics Code

The computer estimate of GDL performance in this experiment was based on the four-temperature kinetics code at AFWL/LRL (Ref 15). In the code, the analysis of the vibrational non-equilibrium inherent in the GDL is done by using vibrational relaxation equations derived from theory and characteristic relaxation times obtained from experiment. The computer program calculates parameters such as the temperatures of the gas, lower and upper laser level, and nitrogen (that is, T , T_1 , T_3 , and T_N) in a finite-difference scheme.

Six equations are solved in an iterative manner at each step through the nozzle; the equations are continuity, conservation of momentum, conservation of energy, and a vibrational relaxation equation for each of the three vibrational temperatures (Ref 13:94). The vibrational relaxation equations are used to find the vibrational temperatures, energies, and population densities. The relaxation equations relate the change of energy of each vibrational mode with its displacement from equilibrium through relaxation times. The relaxation times are inversely proportional to pressure and are strong functions of the temperature (Ref 13:94). The procedure of the code is to first solve the flow equations and then the relaxation equations. The relaxation equations are used to then modify the flow equations results. The process is repeated until T converges to within 0.1 °K; usually one or two iterations are required (Ref 13:94).

Operation of the four-temperature kinetics code required information on the normalized gas composition, stagnation pressure and temperature, and nozzle characteristics such as throat height and area ratio. The code supplied estimates of such parameters as T, T_2 , T_3 , T_N , gain, and energy available for lasing. The calculated variation of the vibrational temperatures with distance from the nozzle throat for three different gas mixtures is shown in Figure 6. The given initial conditions are: $A/A^* = 50$, $h^* = .034$ cm, $T_0 = 2000$ °K, and $P_0 = 500$ psi. It can be seen from the Figure how the gas temperature increases with increasing O_2 content and how T_N ,

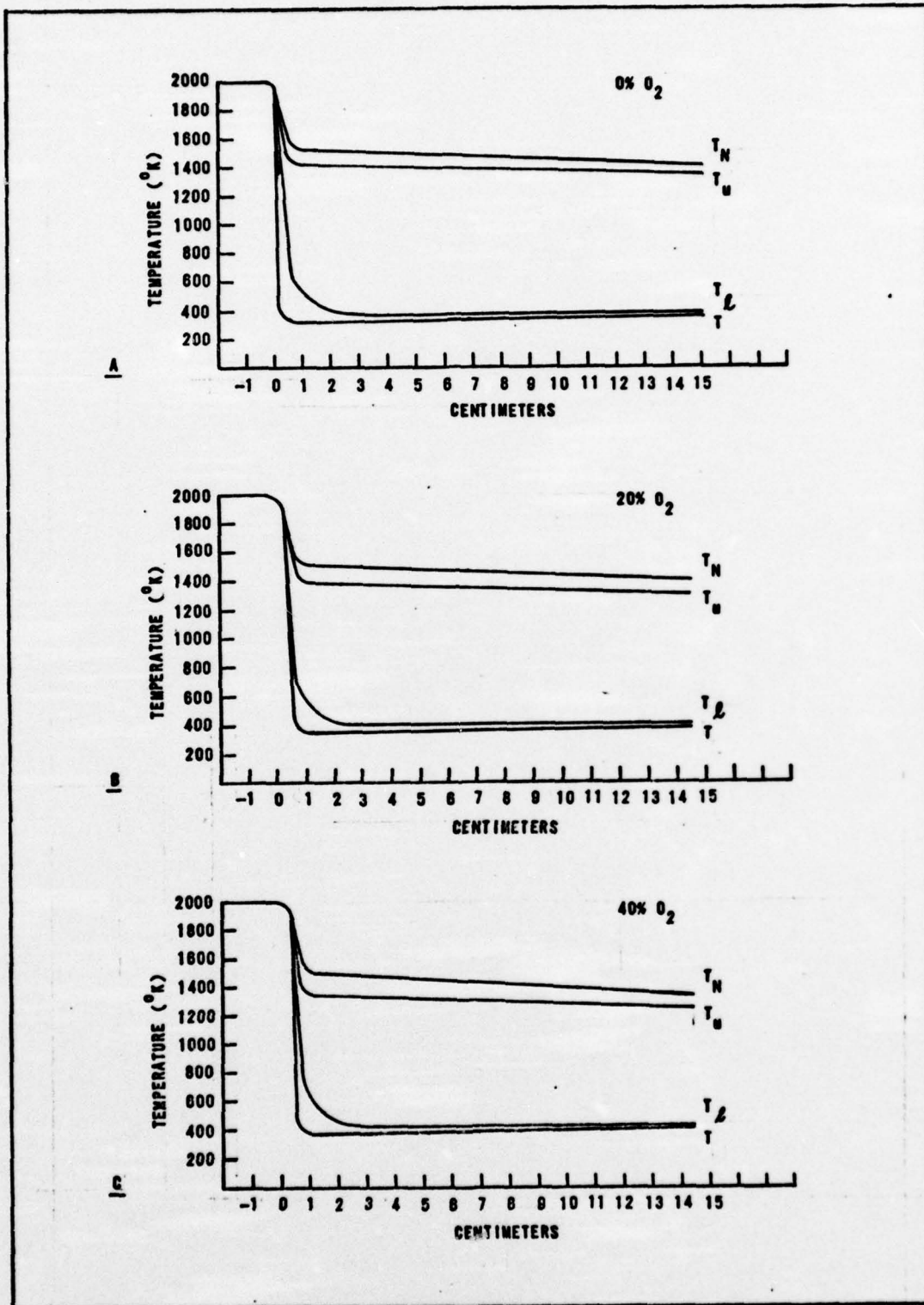


Fig 6. Variation in Temperatures with Distance from Nozzle Throat for Three Gas Compositions.

T_u decrease with increasing O_2 .

J-Line Scan Analysis

The rotational line (J-line) scan technique is a diagnostic method for determining the rotational-translational temperature and the energy available for lasing of the CO_2 -based gas mixture fueling a GDL. A description of a J-line scan method is given in Reference 16. Basically, the technique involves measuring the small-signal gain coefficient at line center on rotational transitions within a branch of, say, the CO_2 (001-100) vibrational transition band. The rotational-translational (or gas) temperature, T , is then deduced from the variation of g with respect to a function dependent upon the rotational transition on which g was measured. The energy available for lasing, E_A , is then determined from the gain and gas temperature.

The J-line scan analysis used in this study differs from the technique outlined in the above reference. Avizonis, et al, made a two-temperature approximation in order to obtain the energy available for lasing. Their approximation then yields a two-temperature value for E_A , and is estimated to be 30% lower than an E_A calculated with a 4-temperature model (Ref 17:30). In this study, the values for T_3 and T were found, and a computer estimate was used to find T_N and T_ℓ . That is, a 4-temperature GDL computer code was used to find the difference between T_N and T_3 and between T_ℓ and T . Knowing these differences and the values for T and T_3 from a J-

line scan, the values of T_N and T can be estimated. These estimates are then used to calculate a 4-temperature E_A . A description of the J-line scan has been published in a note from Flow Research, Inc (#103) by Dr. G. S. Knoke. A brief outline of this method follows.

The Knoke J-line scan method used a different gain equation (at line center) than does Avizonis, et. al. (Ref 18):

$$g = \frac{8\pi^3}{3h\lambda_m} |R|^2 F(m) |m| N_c Q_r^{-1} Q_v^{-1} \phi \quad (6)$$

$$[e^{-\theta_s/T_s} - J_u(J_u + 1)\theta_r/T - e^{-\theta_l/T_l} - J_l(J_l + 1)\theta_r/T]$$

The reader is referred to the list of symbols for the definition of terms in this important equation. Assuming that $\exp(-J_u(J_u + 1)\theta_r/T) = \exp(-J_l(J_l + 1)\theta_r/T)$, Eq (6) becomes:

$$g = \frac{8\pi^3}{3h\lambda_m} |R|^2 F(m) |m| N_c Q_r^{-1} Q_v^{-1} \phi \quad (7)$$

$$[e^{-\theta_s/T_s} - e^{-\theta_l/T_l}] e^{-J_u(J_u + 1)\theta_r/T}$$

Dividing this equation by all terms dependent upon the rotational quantum number (except the exponential term) and dividing by a constant λ_0 ($\lambda_0 = 10.42 \mu$) yields:

$$\frac{\lambda_m}{\lambda_0} \frac{g}{F(m)|m|} = \frac{8\pi^3}{3h\lambda_0} |R|^2 N_c Q_r^{-1} Q_v^{-1} \phi \quad (8)$$

$$[e^{-\theta_s/T_s} - e^{-\theta_l/T_l}] e^{-J_u(J_u + 1)\theta_r/T}$$

for purely collision-broadened lines, $\phi = 2/V_c$ where V_c is the collision frequency for optical broadening; Ref 18 shows:

$$V_c = N_c \left(\frac{8RuT}{\pi} \right)^{1/2} \frac{\sigma(m)}{\sigma_{20}} \left[\sum \frac{\psi_i}{\psi_c} \sigma_{20,i} \left(\frac{1}{m_c} + \frac{1}{m_i} \right)^{1/2} \right] \quad (9)$$

the quantity in brackets varies only with gas composition and can be defined as L . Here, $\sigma_{20,i}$ denotes the optical broadening cross-sections of CO_2 colliding with the i -th species for the transition having the (100) lower laser level and on the P(20) rotational transition. Combining these in Eq (8), and defining $S_j^{-1} = \frac{\lambda_m}{\lambda_0 F(m) |m|}$ gives

$$\frac{\sigma_{jg}}{\sigma_{20} S_j} = \frac{32\pi^3 |R|^2 \theta_r}{3h\lambda_0 \left(\frac{8R_u}{\pi}\right)^{1/2} L} \frac{1}{T^{3/2}} (1 - e^{-\theta_1/T_\ell}) (1 - e^{-\theta_2/T_\ell})^2 (10)$$

$$(1 - e^{-\theta_3/T_3}) (e^{-\theta_3/T_3} - e^{-\theta_\ell/T_\ell}) (e^{-J_u(J_u + 1)\theta_r/T})$$

Taking the ln of Eq (10) yields a straight line in the form $y = b + mx$:

$$\ln \left[\frac{\sigma_{jg}}{\sigma_{20} S_j} \right] = \ln \left[\frac{32\pi^3 |R|^2 \theta_r}{3h\lambda_0 \left(\frac{8R_u}{\pi}\right)^{1/2} L} \left\{ \left(\frac{1}{T^{3/2}} \right) (1 - e^{-\theta_1/T_\ell}) \right. \right. \quad (11)$$

$$\left. \left. (1 - e^{-\theta_2/T_2})^2 (e^{-\theta_3/T_3} - e^{-\theta_\ell/T_\ell}) \right\} (1 - e^{-\theta_3/T_3}) \right] - \frac{\theta_r}{T} J_u(J_u + 1)$$

in the equation above, the y -term of the line is given by $\ln \left[\frac{\sigma_{jg}}{\sigma_{20} S_j} \right]$ and the x -term by $J_u(J_u + 1)$. The gas temperature is found by the slope of the line defined by Eq (11); that is,

$$T = -\theta_r/m = -.56/m \text{ } ^\circ\text{K} \quad (12)$$

Using a four-temperature GDL kinetics code, one can find the differences between the estimated gas temperature and the estimated vibrational temperature of the lower laser level, T_ℓ . The experimental T_ℓ is found by adding the estimated difference of $T_\ell - T$ to the calculated value of T .

The intercept of the line defined by Eq (11), b , with

the ordinate axis yields the vibrational temperature of the asymmetric stretch mode, T_3 . Setting the theoretical and calculated intercepts equal gives:

$$b = \ln \left[\frac{32\pi^3 |R|^2 \theta_r}{3h\lambda_0 \left(\frac{8R_u}{\pi}\right)^{1/2} L} \left(\frac{1}{T^{3/2}}\right) (1 - e^{-\theta_1/T_\ell}) (1 - e^{-\theta_2/T_\ell})^2 \right. \\ \left. (e^{-\theta_3/T_3} - e^{-\theta_\ell/T_\ell}) (1 - e^{-\theta_3/T_3}) \right] \quad (13)$$

Defining $\beta = \frac{3h\lambda_0 L}{32\pi^3 |R|^2 \theta_r} \left(\frac{8R_u}{\pi}\right)^{1/2} T^{3/2} (1 - e^{-\theta_1/T_\ell})^{-1}$
 $(1 - e^{-\theta_2/T_\ell})^{-2} e^b$ and $\delta = e^{-\theta_\ell/T_\ell}$

and substituting in the equation above gives:

$$\beta = (1 - e^{-\theta_3/T_3}) (e^{-\theta_3/T_3} - \delta) \quad (14)$$

or,

$$T_3 = -\theta_3 / \ln \left\{ \frac{1}{2} [(1 + \delta) - \{(1 + \delta)^2 - 4\delta - 4\beta\}^{1/2}] \right\} \quad (15)$$

Thus, values for T , T_ℓ , and T_3 can be found. Once again using a four-temperature code, the estimated value of $T_N - T_3$ can be found. This value is then added to T_3 (determined by the J-line scan) in order to find the experimental T_N .

The energy available for lasing can now be calculated using the following expression (Ref 18):

$$E_A = 3.77 \frac{(\theta_3 - \theta_\ell)}{m} \left[\frac{\psi_{CO_2}}{e^{\theta_3/T_3} - 1} + \frac{\psi_{N_2}}{e^{\theta_N/T_N} - 1} - \frac{\psi_{CO_2} + \psi_{N_2}}{e^{\theta_\ell/T_\ell} - 1} \right] \quad (KJ/lb) \quad (16)$$

where $m = 44\psi_{CO_2} + 18\psi_{H_2O} + 28\psi_{N_2} + 32\psi_{O_2}$.

This expression is for E_A in KJ/lb, on the same branch as the gain was measured.

IV. Experimental Apparatus and Procedure

The problem of making meaningful gain measurements may be broken down into two elements: knowing accurately the composition and thermodynamic condition of the lasing medium, and accurately measuring the gain itself. The first element was determined from a shock tube and its associated gas manifold system. The accurate measurement of gain was made possible by instrumentation probing the test section of the shock tube. It is this apparatus that is discussed in this section.

Shock Tube Facility

This study involved the use of the four-inch shock tube of the Air Force Weapons Laboratory at Kirtland AFB, New Mexico. A description of the AFWL facility is given in Reference 17. The shock tube facility consists of three major components: the shock tube, its associated manifold assembly, and the test section with nozzle array.

Shock Tube. The shock tube is a device used to produce a small reservoir of hot, high-pressure gas. A shock tube consists of a rigid cylinder divided into two sections by a gas tight diaphragm, as shown in Figure 7A. One portion of the tube (the driven section) is evacuated and then filled to a rather low pressure, say, P_1 , with the gas mixture to be studied. The other part of the tube (the driver) is filled with a gas such as He up to a substantially higher pressure, P_4 , which is typically on the order of several hundred psi.

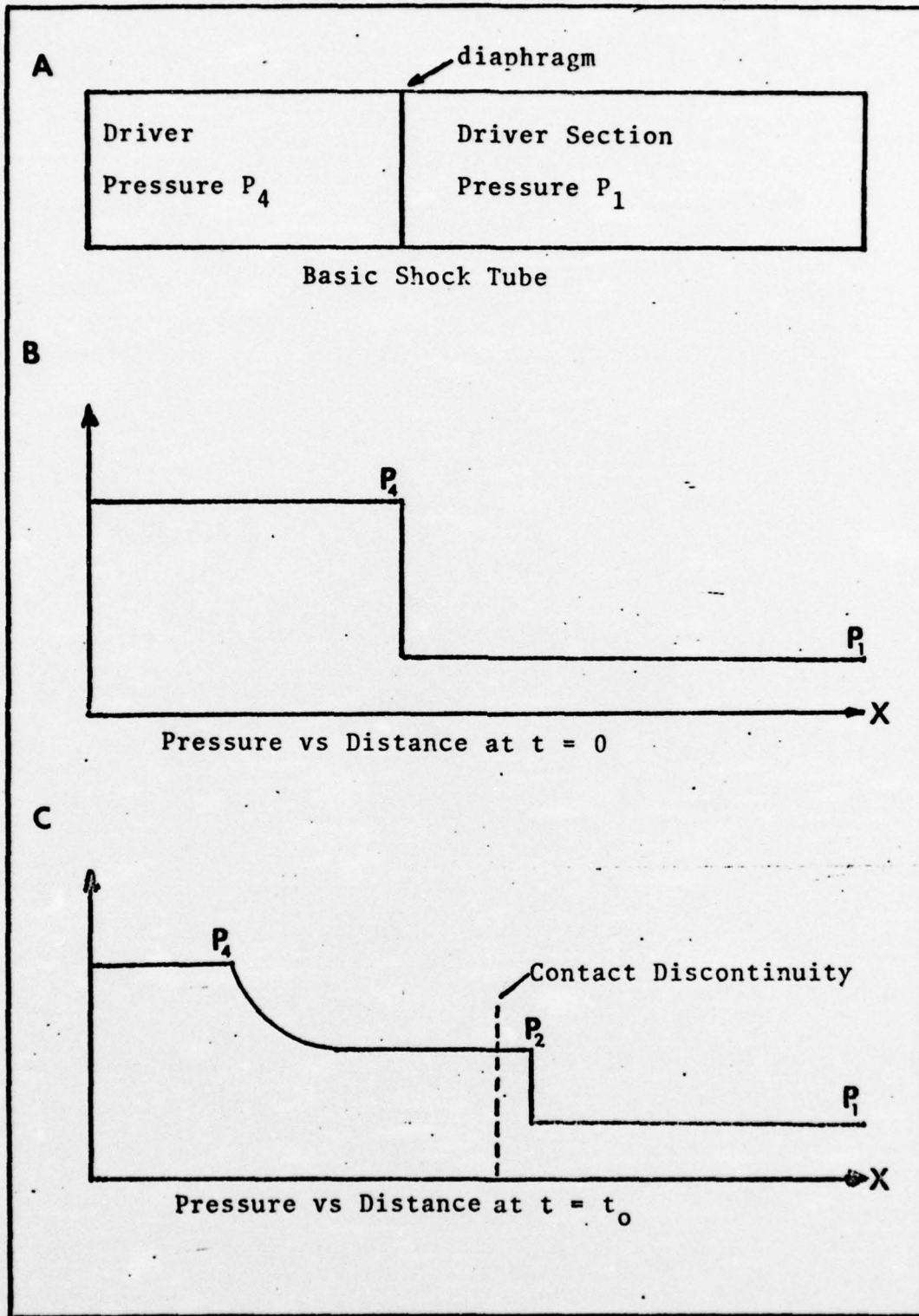


Fig. 7. Shock Tube Schematic (Ref 19:29)

The pressure difference between the two sections of a shock tube is shown in Figure 7B. When the interface separating the driver from the driven section is removed, a shock wave travels into the driven section while a rarefaction wave travels back into the driver gas. Figure 7C depicts the situation in a shock tube just after the diaphragm has shattered. Behind the shock front is a gas flow, and the flow velocity is uniform in the region between the shock front and the tail of the rarefaction wave; this is also a region of constant pressure (Ref 19:30). The dotted line in Figure 7C denotes the position of the two gases that initially were bounded by the diaphragm. The test mixture (to the right) has been compressed and heated, and the driver gas has expanded and hence cooled. The position designated by the dotted line in Figure 7C is called the contact discontinuity (Ref 19:30). Across this line there is, therefore, a change in gas type, temperature, and density; however, the flow velocities are the same on both sides, as in the pressure, P_2 . When the shock wave hits the closed surface at the end of the driven section it is reflected back into the test gas, reheating the mixture and raising the gas pressure still further. Additionally, the expansion fan, upon reflection from the end of the driver section, re-enters the driver and travels down the tube as a rarefaction wave. Figure 8A shows a plot (in the distance versus time plane) of the processes occurring in the shock tube. The shock front position is represented by the line ab. The contact discontinuity is shown by the dotted

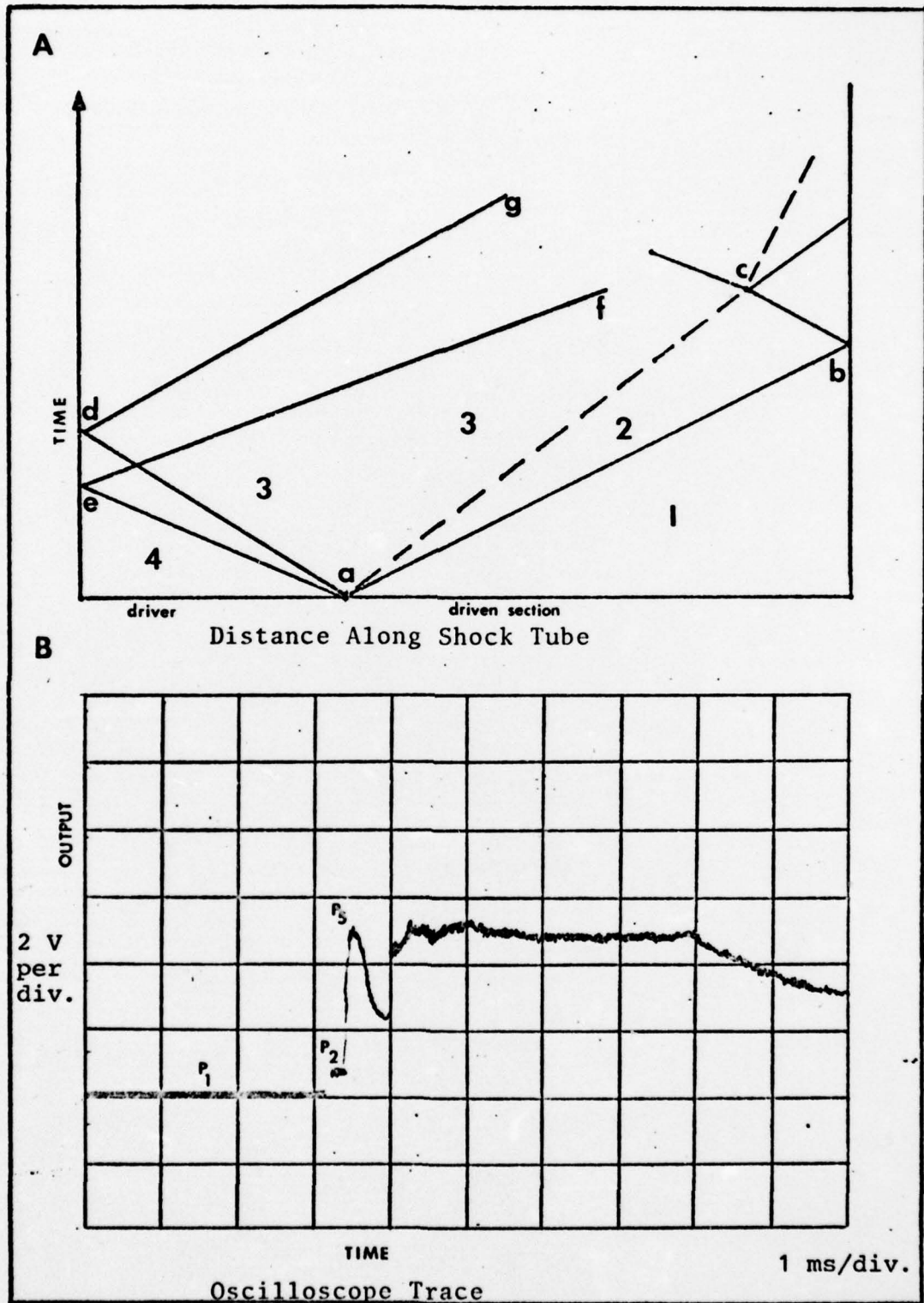


Fig. 8. Pressure Histories in a Shock Tube.

line, ac. This discontinuity meets the shock front at position c.

The shock tube is equipped with two primary diaphragms as well as a secondary diaphragm. The shock tube is constructed of aluminum and is stressed to 2000 psi. The tube has a four-inch inside diameter, the driver section is three meters long, and the driven section is six meters in length.

The primary diaphragms are used to separate the driver from the driven section. Constructed of 1/8"-thick aluminum alloy plates, (alloy #Al-1100-00), the diaphragm plates were scribed

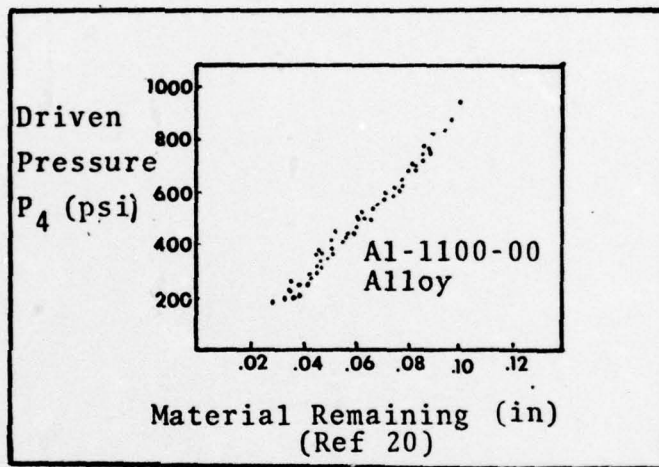


Fig. 9. Diaphragm Pressure Threshold

on a hydraulic press to a specific depth. The thickness of the material remaining in the scribed part of the plates determined their bursting threshold. The relation between breaking pressure and material remaining is shown in Figure 9. Both plates were made to break at a pressure, say P_{th} , such that $P_{4/2} < P_{th} < P_4$. The diaphragms were installed in a manner such that a small volume existed between the upstream and downstream plates. The entire driver (from its downstream diaphragms to its end plate) was filled with He to a pressure a little in excess of $[P_4]/2$. The small chamber

separating the two diaphragms was then closed off from the major portion of the driver. The remainder of the driver was then filled to the desired P_4 value. The shock tube was fired by venting off the pressurized He in the small chamber, thus meeting the pressure thresholds on both diaphragms. This dual-diaphragm system permitted accurate and repeatable stagnation conditions (T_5 and P_5), exceeding the accuracy available from a single-diaphragm system. By using the dual-diaphragm system, shock speeds were repeatable to within 2%, and desired T_5 values were easily repeated to within ± 50 °K (Ref 21:139). Beside the two primary diaphragms, a small (1/16"-thick) scribed aluminum plate was mounted on the end of the driven section. Designed to break at about 16 psi, this secondary diaphragm served to seal off the driven section at pressure P_1 from the evacuated test section (containing the GDL nozzles). It should be noted that for all tests on the shock tube, the driven section and the test cell were evacuated to at least 250 microns pressure, and usually to less than 150 microns.

Once the driver section was sealed off and evacuated from the test section, the test gas was added to the driven cell. When the shock wave travels through the test mixture it raises the pressure of the gas to P_2 . Figure 8 B shows a reproduction of an actual pressure versus time trace of the events occurring in the AFWL shock tube during a typical test. Two quartz piezoelectric pressure transducers were mounted at the end of the driver section, and their outputs were amplified. The output from the upstream transducer initiated a

timer as well as the sweep on the oscilloscope. The output from the downstream transducer is shown in the Figure. As is shown, the test gas initially remains at pressure P_1 until the shock wave traverses through the mixture, increasing the pressure to P_2 . The shock wave reflects off the secondary diaphragm, rupturing the plate and reheating the gas. The pressure of the gas is raised to P_5 , which rapidly decays to a lower value as the diaphragm breaks and as the mixture expands into the volume originally enclosed by the position of the secondary diaphragm and the nozzle entrance plane (in the test section). The pressure then rises to P_5 again, and it is now that gain measurements are made. For what is termed a well-tailored driver gas, the pressure trace tends to be fairly level; this permits a useful test time of up to 3 ms. The test time is destroyed, however, as the expansion fan interacts with the reflected shock wave. The expansion wave lowers the gas pressure and temperature, as can be seen in Figure 8 B.

Experiments were performed for stagnation temperatures of 1950 to 2050 °K and stagnation pressures of 480 to 520 psi. The stagnation temperature is calculated from normal shock relationships, using the computer estimate provided by AFWL (Ref 22), experimentally-found values for the stagnation pressure, and the measured shock wave speed. The computer estimate of the stagnation temperature, is similar to a published code, developed by Madden (Ref 23).

Manifold Assembly. The gas manifold associated with the

AFWL shock tube was used for mixing test gases as well as a 4% CO₂, 14% N, Balance He mixture required for the diagnostic CO₂ laser. A photograph of the manifold and its accompanying gauge panel is shown in Figure 10. In the photograph, the left-hand gauge, a Heise 0 to 3000 psia pressure gauge, monitored the pressure in the driver. Immediately to the right of the driver gauge is a Heise 0 to 800 torr vacuum gauge. Connected to this gauge is a Varian electric vacuum gauge (1 atm to 0 microns), shown at the top of the panel. These two vacuum gauges monitored the vacuum in the driven section prior to filling the section with test gas. The two Heise gauges (0 to 500 and 0 to 3000 psi) on the lower right-hand side of the panel monitored the manifold pressure. The various valves on the panel were used to isolate the vacuum gauges from the driven section immediately prior to firing the shock tube, and for venting and blow-off purposes.

The manifold permitted such gases as CO₂, H₂, N₂, and O₂ to be mixed in different combinations to a variety of pressures. In mixing test gases, the manifold and the test gas storage bottles (stainless steel) were evacuated to typically 100 microns. The gases of lowest percentage would be filled first to insure accuracy in gas mixture composition. Upon filling the storage bottles to the desired pressure, the bottles were closed off and the manifold vented. The storage bottles were then warmed with an electric heat gun for 5 to 10 minutes and allowed to cool for 30 minutes to insure mixing was complete. The pressure to which the bottles were filled

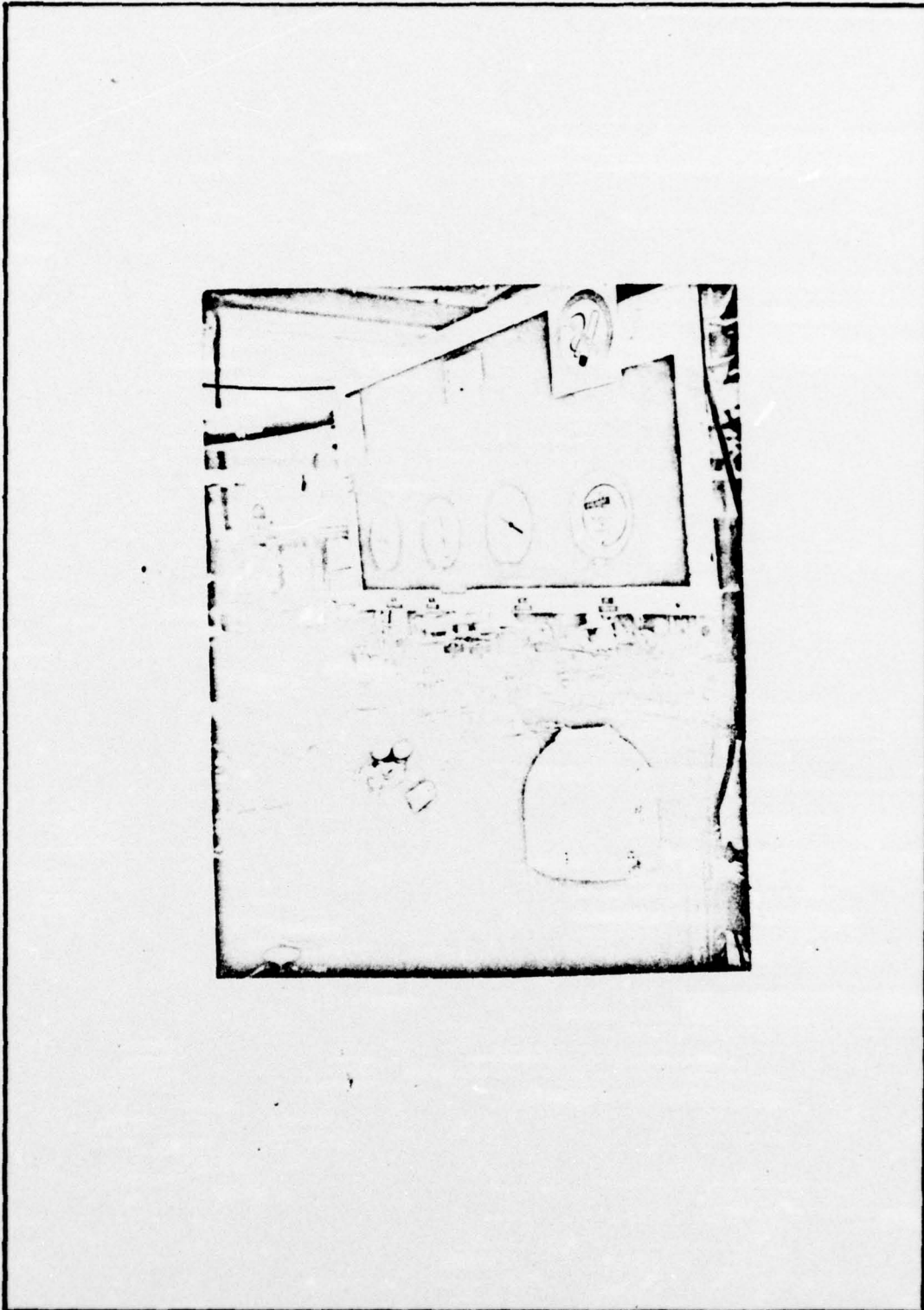


Fig.10. Shock Tube Gas Manifold Assembly.

varied with the gas mixture. The 0% oxygen excess mixture (10%CO₂, 3%H₂O, Bal N₂) was pressurized in the bottles to 500 psia. The 10% oxygen mixture was filled to 400 psi, 20% excess O₂ to 250 psi, 30% O₂ to 175 psi and 40% excess O₂ to 100 psi. After the test gases were mixed, the storage bottles were opened and the driven section was filled, using various valves and gauges on the manifold panel. The driven section was typically filled to a pressure of about 4 psia, and the driver section was filled with He to a pressure around 800 or 900 psia.

Nozzle Array and Test Section. A seven-element nozzle array was used in the performance of this experiment. The nozzle array, securely housed in a test cell, was located immediately upstream of three ports drilled into the test section. The grid nozzle array was made in the form of an integral assembly, with the beryllium nozzle elements welded into position and retained in the copper holder. The area ratio of the nozzles was measured for each pair of nozzles and the total was averaged over the multi-nozzle set. The throat height, h^* , was measured and likewise averaged over the array. The average values for A/A^* and h^* were found to be 53 and .034 cm, respectively. Additional nozzle array data can be found in the Appendix. The test section which housed the nozzle array was constructed of aluminum and connected the shock tube to the dump tank. Three sets of 6.6 cm diameter viewing ports were located immediately downstream of the nozzle exit plane; the first set was centered 3.6 cm downstream of the nozzle exit plane and was centered 8.0 cm downstream of the

nozzle throat, the second about 15 cm downstream of the throat, and the third was 21 cm downstream of the nozzle throats. Only the first set of ports was used; the downstream sets were plugged with aluminum fillers. Gain measurements were made in the expanded gas downstream from the nozzles through the 12.7 cm wide test section. The optical path of the diagnostic laser beam passed through the pair of germanium windows, which were 2" in diameter and .25" thick. The windows were placed in an aluminum retainer, using an O-ring, and each retainer was bolted into the test section. A schematic of the test section is shown in the Appendix.

Gain Measurement

Finding the energy available for lasing of a particular mixture implies that the critical element in the experiment is the accurate measurement of the small-signal gain coefficient obtained from the test gas. The apparatus used to measure the gain is depicted in Figure 11. The most important component of the measurement apparatus was the CO₂ diagnostic laser. This laser had to meet two criteria: it had to be tunable from the P(12) to P(30) transitions of the 10.6 μ band, and it had to exhibit stability on those transitions. The laser most often used in this experiment was a Coherent Radiation Model 42 industrial CO₂ laser. The power output of this laser was typically around 20 watts on the P(20) transition with decreasing power on other P-branch lines. Although there was more than an ample amount of power avail-

able from the Model 42 laser, its beam quality was poor, it was difficult to maintain lasing in the TEM_{00} mode, indeed, it tended to lase in the TEM_{10} mode. The laser had to be 'peaked' prior to each test due to the high noise level inherent in the signal from the laser whenever it operated below its optimum output. Another drawback of this laser was that it was a flowing gas system instead of a sealed tube configuration. The flowing gas necessitated refilling the laser gas bottle almost every day. Still another detrimental feature of the laser was that it was large and bulky. Considering the components of the system-laser head, control unit, refrigeration unit, and laser gas bottle - this laser required quite a bit of room. Finally, the Model 42 was not nearly as stable as another laser which was used in this experiment. This other laser was a 1976 Sylvania 950 A/B. This Sylvania CO_2 laser was the first laser off the assembly line that was equipped with a new model power supply. The power output of this laser was around seven watts, much lower than the Coherent Radiation laser but ample for this experiment. After the initial warm-up period, the Sylvania 950 operated in the TEM_{00} mode consistently. This laser had a sealed tube of laser gas. The sealed tube laser was more compact and much less bulky than the 20-watt laser. However, even though the Sylvania 950 was more desirable of the two lasers used, the new power supply failed after a week of service and the laser, its power supply (as well as another supply - the third off of the assembly line) had to be replaced

after arcing developed in the high voltage module of the laser head. The Coherent Radiation industrial laser was once again used as the diagnostic laser following the failure of the Sylvania 950 A/B.

Although the probe laser is the single most important piece of equipment of the measurement apparatus, other devices were required to complete the apparatus. Figure 11 shows schematically the layout of the apparatus on the air table. The probe beam was directed on a straight-line path to a beam steerer which reflected the laser radiation 90 degrees into the test section. The beam steerer was equipped with two elliptical mirrors that provided 99% reflectance of 10.6μ illumination. After being turned by the beam steerer, the probe radiation illuminated the first of two .25 inch diameter apertures. This first aperture served to reduce considerably the amount of radiation entering downstream components on the air table. Upon exiting the first aperture, the beam was irregularly interrupted at intervals in the order of one Khz by a beam chopper. The chopped beam was then fell incident upon a flat germanium 50-50 beam splitter. One part of the incident radiation was transmitted through the beam splitter and continued into the test section windows. The reflected part of the beam was directed onto the slit of a CO_2 spectrum analyzer; the spectrum analyzer served to provide definitive information as to which P-branch transition the probe laser was operating on. Further, the calibration of the spectrum analyzer was checked at the beginning of the experiment with a

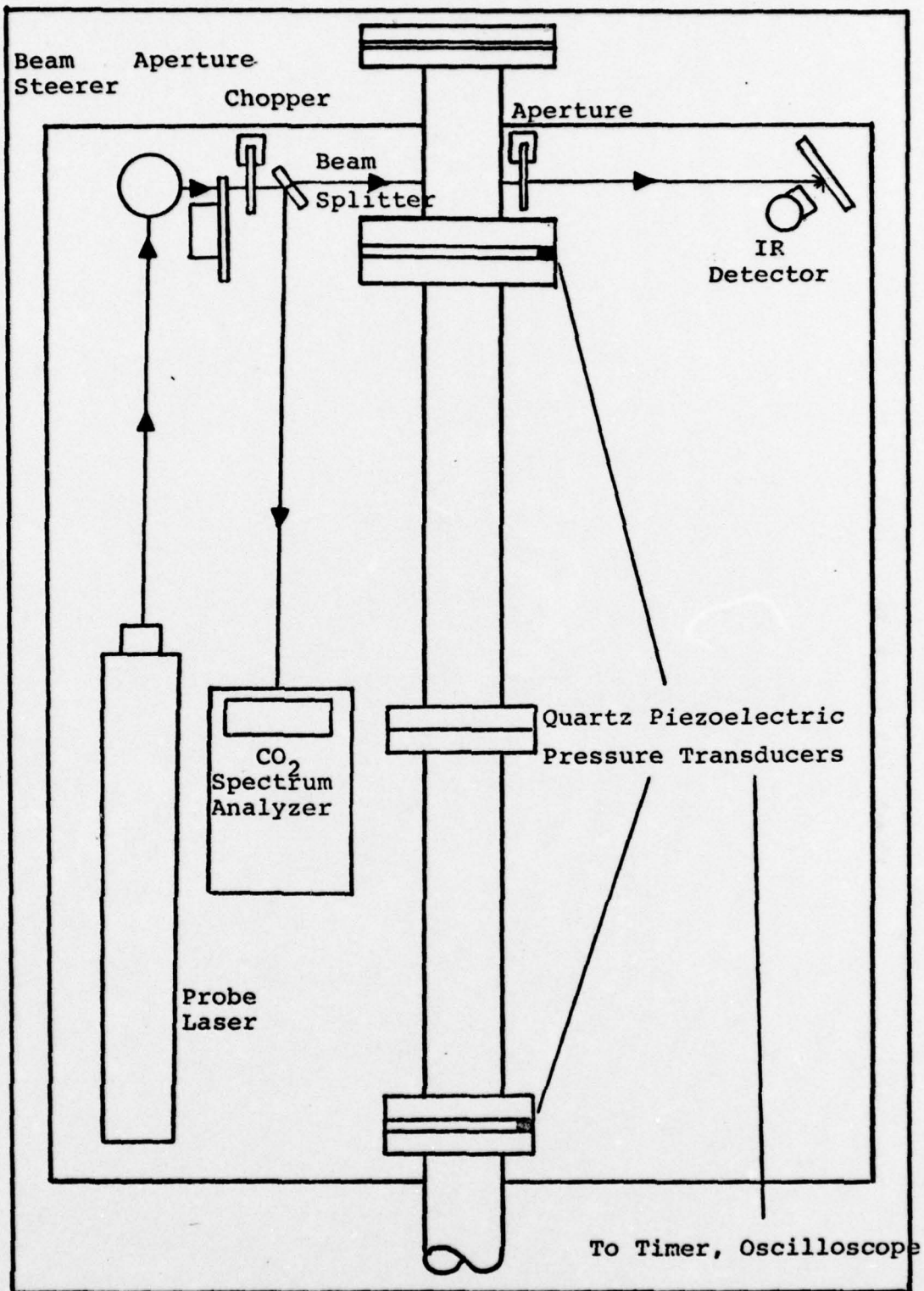


Fig. 11. Schematic of Experimental Apparatus.

known source. While the reflected portion of the beam terminated at the spectrum analyzer, the transmitted beam illuminated the first germanium window of the test section. This first window had an anti-reflection coating in order to reduce any backscattered irradiation on the diagnostic laser. After exiting the second germanium window directly across the 12.7 cm length of test section, the beam was once again apertured. The purpose of the second aperture was to reduce any spurious IR radiation. A notable source of such spurious illumination would be the 4.3μ radiation resulting from the (001) to (000) transition of CO_2 . The apertured IR beam then illuminated the diffuse surface of a sandblasted aluminum plate. The final component of the experimental apparatus, the IR detector, was placed directly opposite (and pointed at) the illuminated area on the sandblasted plate. The IR detector, equipped with a 10.6 bandpass interference filter, employed a HgCdTe chip with an active detector area of $2.6 \times 10^{-3} \text{ cm}^2$. The IR detector was maintained at 77 °K throughout the experiment. One disadvantage of this detector was that its dewar required evacuation every two or three days in order to prevent excessive liquid N_2 boiloff. Figure 12 is a photograph of the experimental apparatus of this experiment.

A Tektronix model 7904 oscilloscope was used to monitor both the probe beam as well as the pressure trace from the shock tube transducers. The oscilloscope is triggered such that the shock front, incident upon the upstream pressure

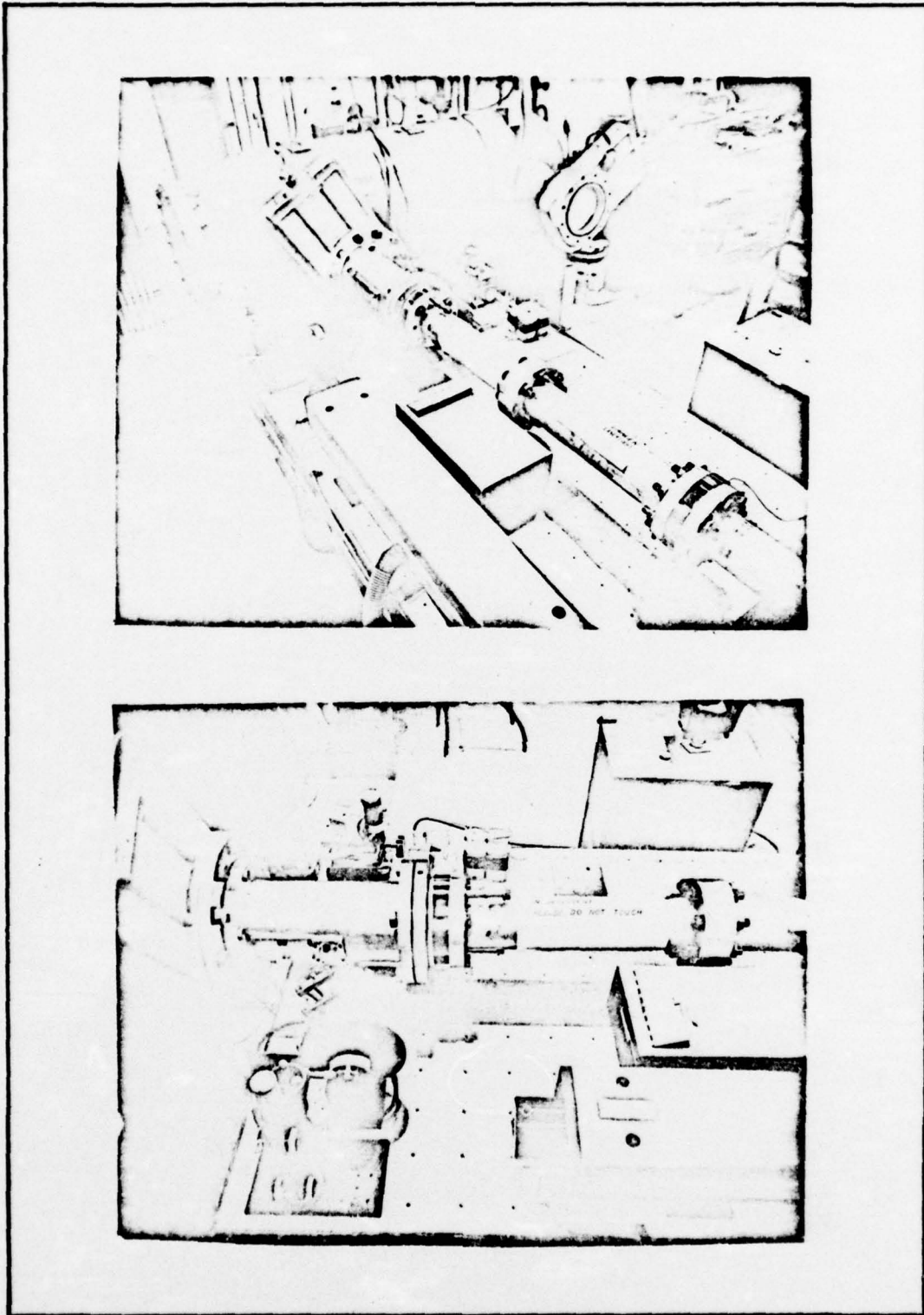


Fig. 12. Photographs of Experimental Apparatus.

transducer, initiated the trace. This triggering scheme permits determination of the probe laser intensity for both flow (I_V) and no-flow ($I_V + \Delta I_V$) environments in the test section. The gain is measured directly from an oscillogram upon completion of a test on the shock tube. A typical oscillogram is shown in Figure 13. The pressure P_0 in the figure corresponds to the stagnation pressure P_5 discussed earlier. As can be inferred from the figure, the increase in IR radiation indicates the presence of an amplifying medium (and this gain is equal to ΔI_V), where the incident radiation is I_V .

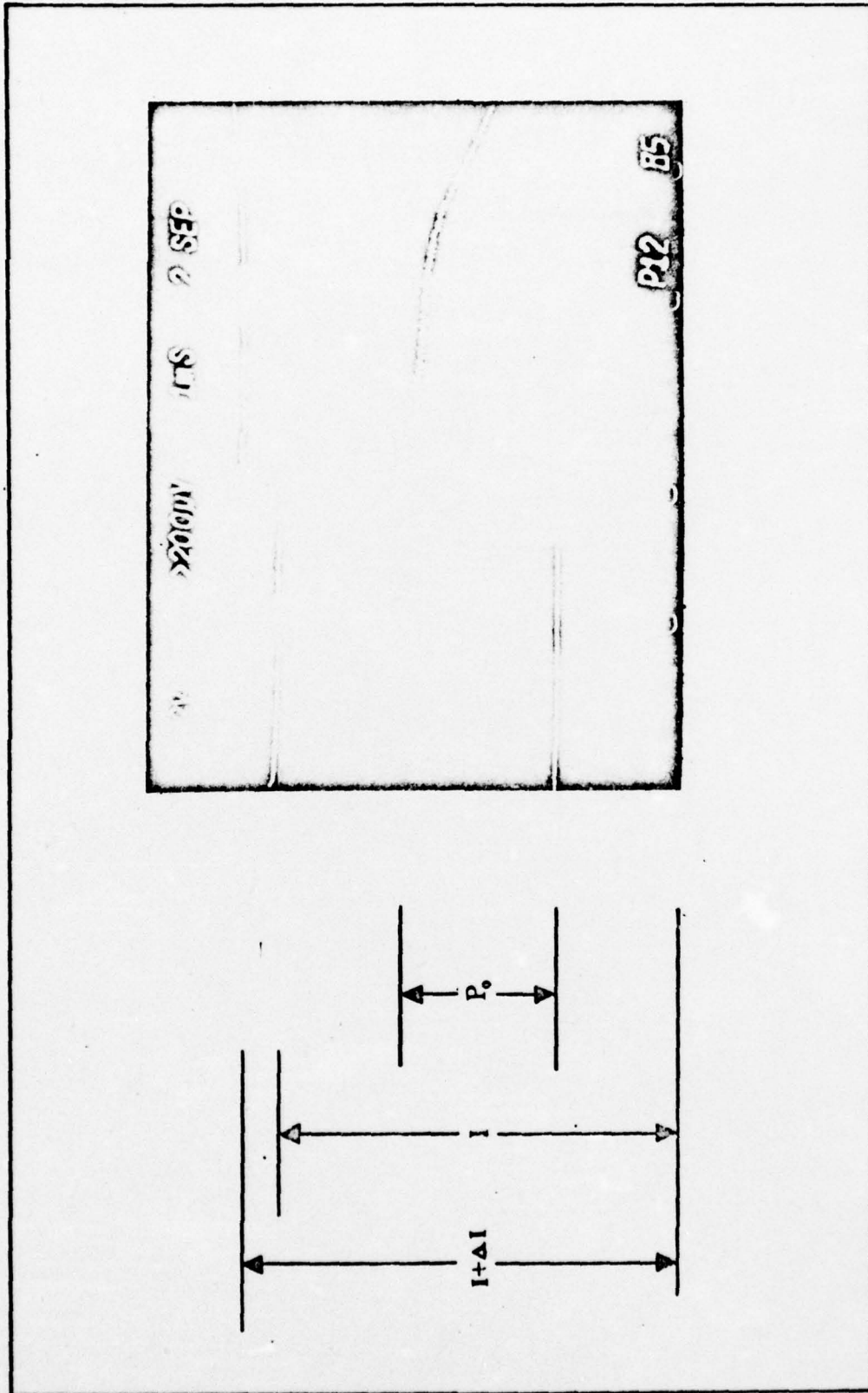


Fig. 13. Oscillogram from which Gain Measurement is Made.

V. Results and Discussion

Presentation of Data

The effect upon energy available for lasing and upon the small-signal gain coefficient of different lasing media was studied as O_2 replaced the N_2 content of test gases fueling a GDL. The interest in O_2 comes about from its abundance in the fuel mixtures of third-generation devices; i.e., bireactant gas dynamic lasers. The small-signal gain coefficient pertaining to each test gas was measured four times on each of three P-branch transitions. The raw gain data obtained from these measurements is presented in Appendix A. Once the gain measurement series was completed for each test mixture, a J-line scan analysis was used to reduce the data. The J-line scan technique yielded values for T , T_3 , and E_A .

Reduced data is presented in this section in sets of three in the following manner. The first table of each set shows the experimental results obtained from a particular gas composition as well as calculated J-line scan information. Immediately following the first table is a graph on which the experimentally-derived values of $\ln \left[\frac{\sigma_j}{\sigma_{20} s_j} \right]$ and $J_u (J_u + 1)$ are plotted. Also plotted on each graph is a least-squares fit of the data points. On the page subsequent to each graph is a second table which shows the interpolated value of gain on each of seven rotational transitions. These interpolated results were found from a

linear regression technique, using the least-squares line as a basis. Also presented in the Interpolated Results Tables are calculated values for the intercept of the least-squares fit, its slope, and consequently the gas temperature of the test mixture. As described earlier, once the intercept of the least-squares line and the gas temperature are known, the vibrational temperature of the upper laser level can be calculated. Then, using computer estimates of $T_N - T_3$ and of $T_1 - T$, one can find values for T_N and T_1 . The calculated values of T, T_1, T_3 , and T_N are in turn used to determine E_A for each test gas.

Results

Baseline Case. The first set of reduced data pertains to the test gas composed of 10% CO_2 , 87% N_2 and 3% H_2O . The gain was measured on the P(12), P(18), and P(30) transitions, as shown in Table I. Figure 14 shows the distinct linear relation between the logarithmic term and the rotational quantum number function, in accordance with theory. The error bar shown was deduced by assuming a 5% error in gain measurements. With the assumption of this liberal 5% error, Table II shows the gas temperature and intercept.

Ten Percent Excess O_2 . The second set of data is from the test gas comprised of 10% CO_2 , 77% N_2 , 3% H_2O , and 10% O_2 . Once again, the experimental results are shown on the first of the tables, the J-line scan is plotted on the graph, and the interpolated values are calculated on the following table.

Table I
 Experimental Results
 0% Oxygen Contamination

P Line	$J_u (J_u + 1)$	$g \text{ (cm}^{-1}\text{)}$	$\frac{\sigma_{20} s_J}{\sigma_J}$	$\ln \left(\frac{\sigma_J g}{\sigma_{20} s_J} \right)$
12	132	.0075	11.3	-7.32
12	132	.0075	11.3	-7.32
12	132	.0076	11.3	-7.30
12	132	.0078	11.3	-7.28
18	306	.0088	17.5	-7.59
18	306	.0090	17.5	-7.57
18	306	.0091	17.5	-7.56
18	306	.0092	17.5	-7.55
30	870	.0071	30.5	-8.36
30	870	.0072	30.5	-8.35
30	870	.0072	30.5	-8.35
30	870	.0074	30.5	-8.32

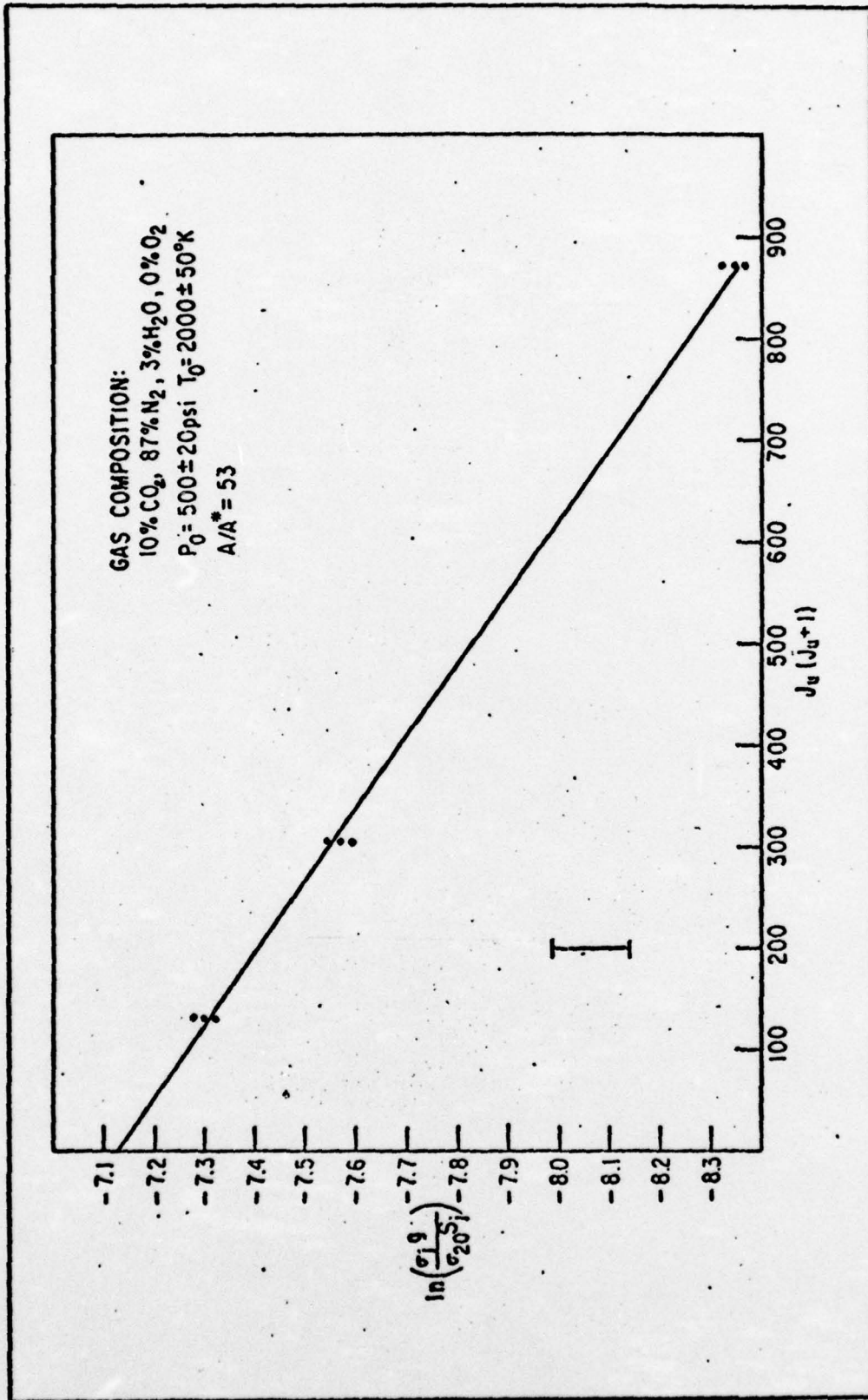


Fig. 14. J-Line Scan: 0% O₂ Case

Table II
Interpolated Results
0% Oxygen Contamination

P Line	$J_u(J_u + 1)$	$\frac{\sigma_{20} s_j}{\sigma_j}$	$\ln \left(\frac{\sigma_j g}{\sigma_{20} s_j} \right)$	$g \text{ (cm}^{-1}\text{)}$
12	132	11.3	-7.31	.0076
16	240	15.4	-7.46	.0089
18	306	17.5	-7.56	.0091
20	380	19.6	-7.66	.0092
22	462	21.7	-7.78	.0091
24	552	23.9	-7.90	.0089
30	870	30.5	-8.35	.0072

Slope = -0.001402

Intercept = -7.13

Gas Temperature = 399 °K

Table III
 Experimental Results
 10% Oxygen Contamination

P Line	$J_u (J_u + 1)$	$g \text{ (cm}^{-1}\text{)}$	$\frac{\sigma_{20} s_j}{\sigma_j}$	$\ln \left(\frac{\sigma_j g}{\sigma_{20} s_j} \right)$
12	132	.0062	11.3	-7.51
12	132	.0063	11.3	-7.49
12	132	.0063	11.3	-7.49
12	132	.0064	11.3	-7.48
20	380	.0076	19.6	-7.85
20	380	.0078	19.6	-7.83
20	380	.0078	19.6	-7.83
20	380	.0079	19.6	-7.82
30	870	.0060	30.5	-8.53
30	870	.0061	30.5	-8.51
30	870	.0062	30.5	-8.50
30	870	.0063	30.5	-8.48

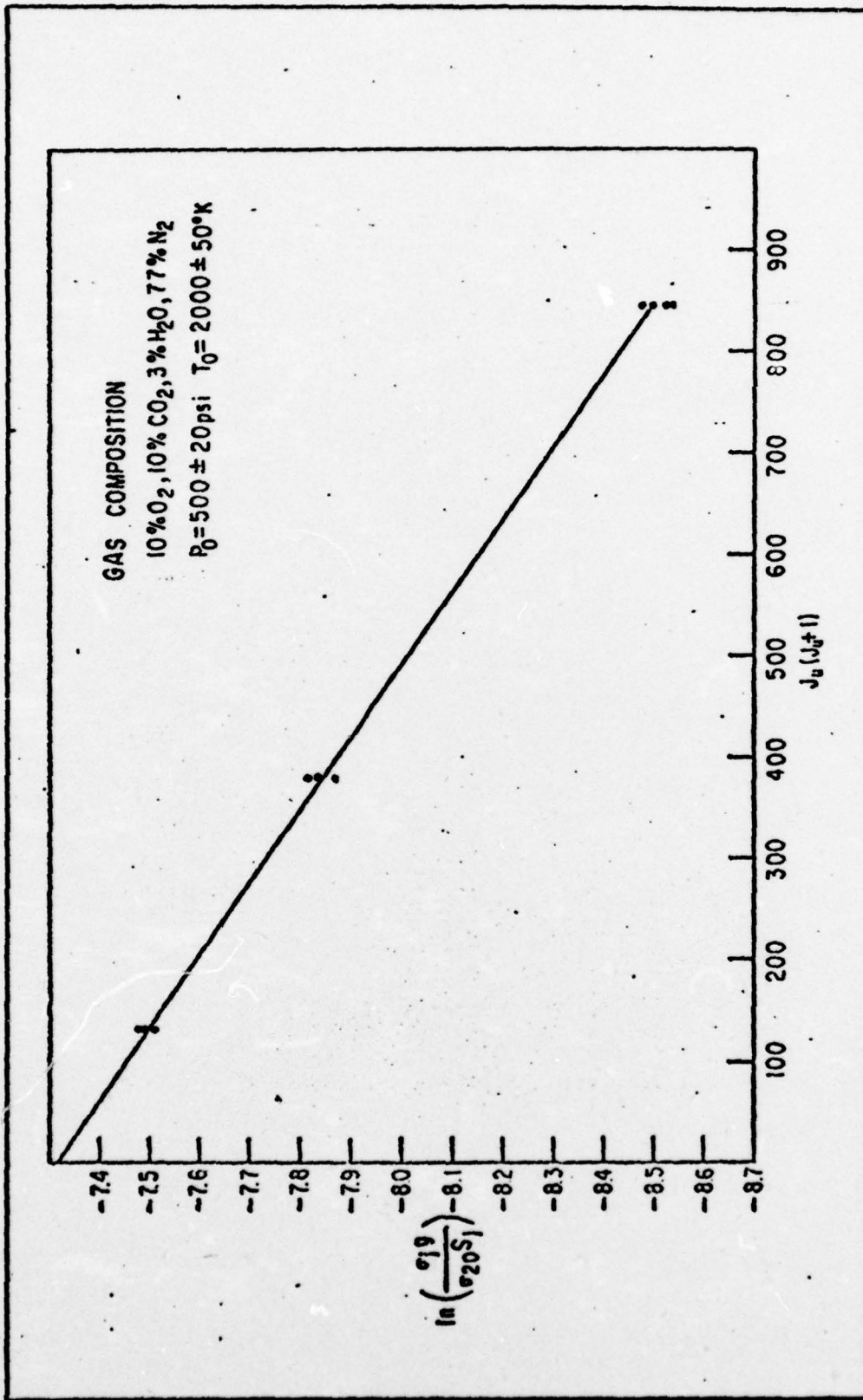


Fig. 15. J-Line Scan: 10% O₂ Case

Table IV
Interpolated Results
10% Oxygen Contamination

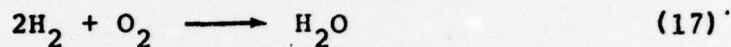
P Line	$J_u(J_u + 1)$	$\frac{\sigma_{20} s_j}{\sigma_j}$	$\ln \left(\frac{\sigma_j g}{\sigma_{20} s_j} \right)$	$g \text{ (cm}^{-1}\text{)}$
12	132	11.3	-7.49	.0063
16	240	15.4	-7.64	.0074
18	306	17.5	-7.73	.0077
20	380	19.6	-7.83	.0078
22	462	21.7	-7.94	.0077
24	552	23.9	-8.07	.0075
30	870	30.5	-8.50	.0062

Slope = -0.001372

Intercept = -7.31

Gas Temperature = 408 °K

Other Excess O₂ Mixtures. The following tables and graphs incorporate the reduced data from the remaining gas compositions, and follow the same format as outlined above. In all cases, the gas mixture was composed of 10% CO₂, 3% H₂O, and X% O₂, with the balance being made up by N₂. In all test mixtures, water was produced through the process



Discussion

Effect of O₂ on T, T₁. Oxygen replacement of the N₂ content of the test gas causes an increase in the gas temperature as well as a consequent increase in the vibrational temperature of the upper laser level. As shown in Figure 19, the heat addition in the gas temperature amounts to about 0.2% for each percent of excess O₂ present in the mixture. As indicated in Eq (5), excited O₂ is readily deactivated by H₂O. This kinetic reaction is exothermic, and the subsequent temperature rise is expected. The presence of H₂O also serves to deactivate the lower laser level; unplugging this bottleneck tends to allow this level to equilibrate with the gas temperature. However, the equilibration of T and T₁ is not complete 8 cm downstream of the nozzle throats, where the data was taken. As the Figure shows, there exists a difference between T and T₁, though diminishing with distance, of about 20°K. The tendency of the vibrational temperature of the upper laser level to

Table V
 Experimental Results
 20% Oxygen Contamination

P Line	$J_u (J_u + 1)$	$g \text{ (cm}^{-1}\text{)}$	$\frac{\sigma_{20} S_J}{\sigma_J}$	$\ln \left(\frac{\sigma_J g}{\sigma_{20} S_J} \right)$
12	132	.0054	11.3	-7.65
12	132	.0056	11.3	-7.61
12	132	.0056	11.3	-7.61
12	132	.0058	11.3	-7.57
20	380	.0071	19.6	-7.92
20	380	.0072	19.6	-7.91
20	380	.0076	19.6	-7.85
20	380	.0076	19.6	-7.85
30	870	.0054	30.5	-8.64
30	870	.0055	30.5	-8.62
30	870	.0059	30.5	-8.55
30	870	.0059	30.5	-8.55

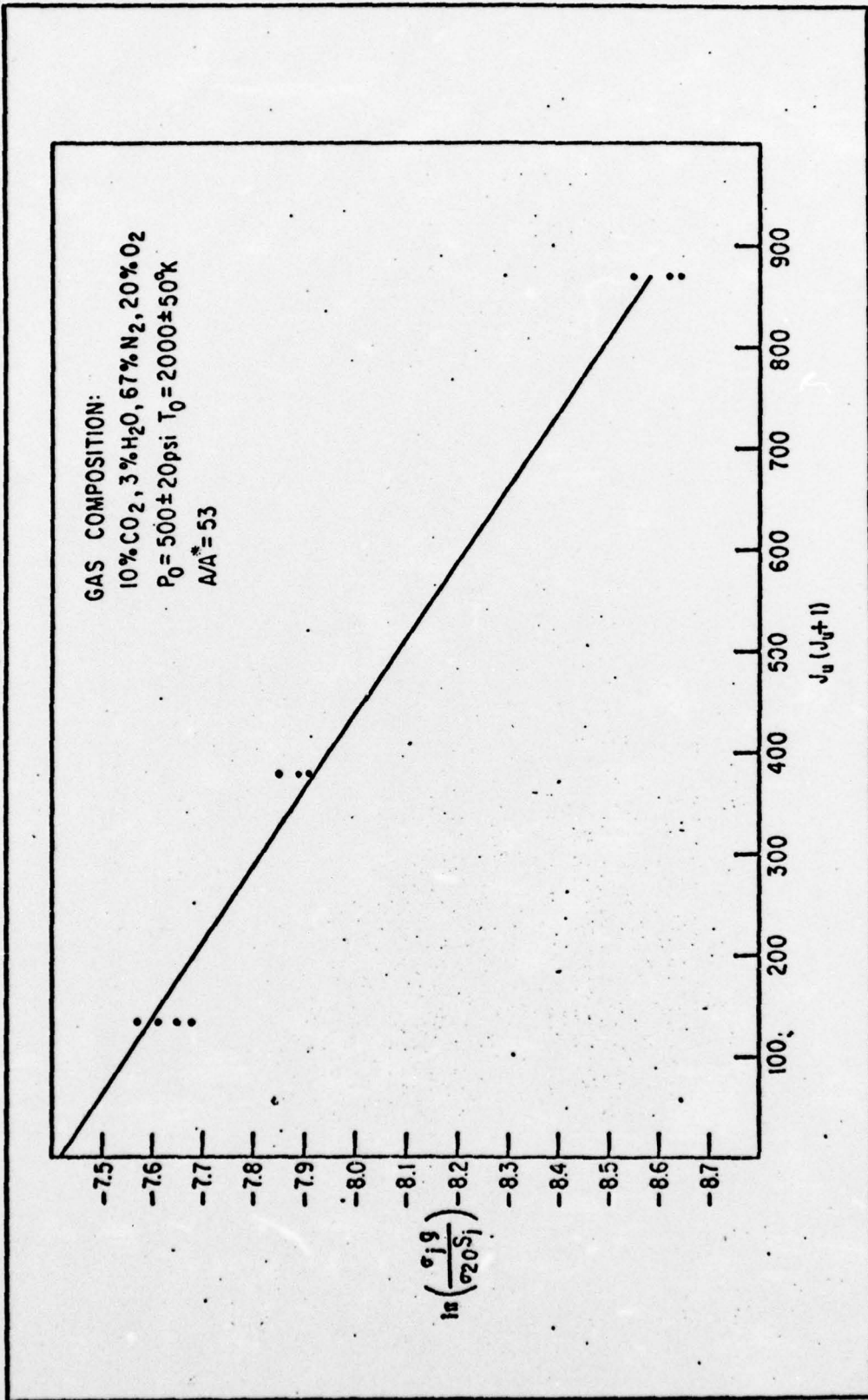


Fig. 16. J-Line Scan: 20% O₂ Case

Table VI
Interpolated Results
20% Oxygen Contamination

P Line	$J_u(J_u + 1)$	$\frac{\sigma_{20} s_j}{\sigma_j}$	$\ln \left(\frac{\sigma_j g}{\sigma_{20} s_j} \right)$	$g \text{ (cm}^{-1}\text{)}$
12	132	11.3	-7.59	.0057
16	240	15.4	-7.73	.0068
18	306	17.5	-7.82	.0070
20	380	19.6	-7.92	.0071
22	462	21.7	-8.03	.0071
24	552	23.9	-8.15	.0069
30	870	30.5	-8.58	.0057

Slope = -0.001344

Intercept = -7.41

Gas Temperature = 417 °K

Table VII
 Experimental Results
 30% Oxygen Contamination

P Line	$J_u (J_u + 1)$	$g \text{ (cm}^{-1}\text{)}$	$\frac{\sigma_{20} s_j}{\sigma_j}$	$\ln \left(\frac{\sigma_j g}{\sigma_{20} s_j} \right)$
12	132	.0051	11.3	-7.70
12	132	.0052	11.3	-7.68
12	132	.0053	11.3	-7.66
12	132	.0055	11.3	-7.63
20	380	.0066	19.6	-8.00
20	380	.0066	19.6	-8.00
20	380	.0067	19.6	-7.98
20	380	.0067	19.6	-7.98
30	870	.0050	30.5	-8.72
30	870	.0053	30.5	-8.66
30	870	.0055	30.5	-8.62
30	870	.0056	30.5	-8.60

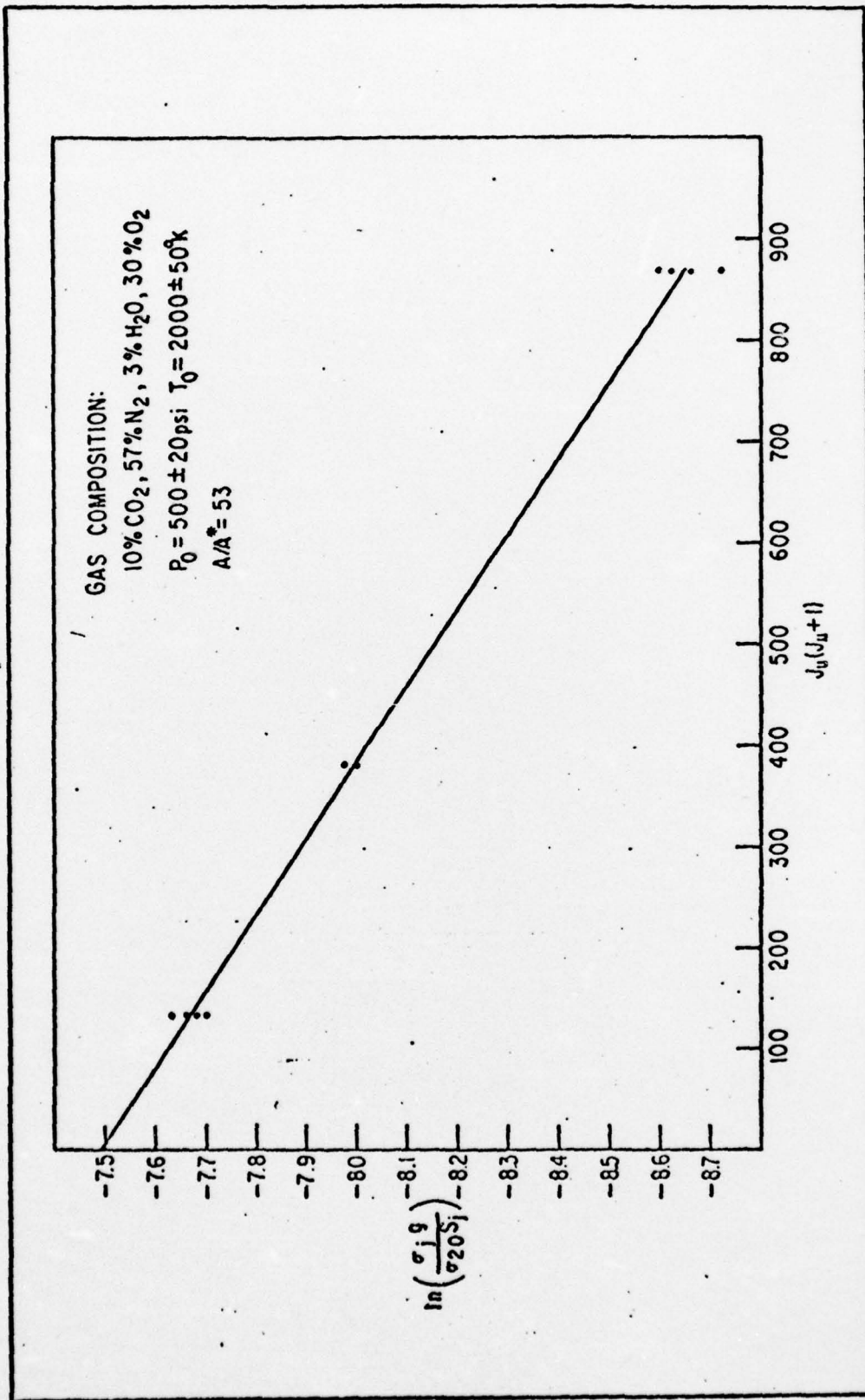


Fig. 17. J-Line Scan: 30% O₂ Case

Table VII
Interpolated Results
30% Oxygen Contamination

P Line	$J_u(J_u + 1)$	$\frac{\sigma_{20} s_j}{\sigma_j}$	$\ln \left(\frac{\sigma_j g}{\sigma_{20} s_j} \right)$	$g \text{ (cm}^{-1}\text{)}$
			.	
12	132	11.3	-7.66	.0053
16	240	15.4	-7.81	.0062
18	306	17.5	-7.90	.0065
20	380	19.6	-7.99	.0066
22	462	21.7	-8.10	.0066
24	552	23.9	-8.22	.0064
30	870	30.5	-8.65	.0053

Slope = -0.001333

Intercept = -7.49

Gas Temperature = 420 °K

Table IX
 Experimental Results
 40% Oxygen Contamination

P Line	$J_u (J_u + 1)$	$g \text{ (cm}^{-1}\text{)}$	$\frac{\sigma_{20} s_J}{\sigma_J}$	$\ln \left(\frac{\sigma_J g}{\sigma_{20} s_J} \right)$
12	152	.0041	11.3	-7.92
12	132	.0041	11.3	-7.92
12	132	.0042	11.3	-7.90
12	152	.0044	11.3	-7.85
18	306	.0047	17.5	-8.20
18	306	.0050	17.5	-8.16
18	306	.0052	17.5	-8.12
18	306	.0052	17.5	-8.12
30	870	.0042	30.5	-8.89
30	870	.0043	30.5	-8.87
30	870	.0044	30.5	-8.84
30	870	.0045	30.5	-8.82

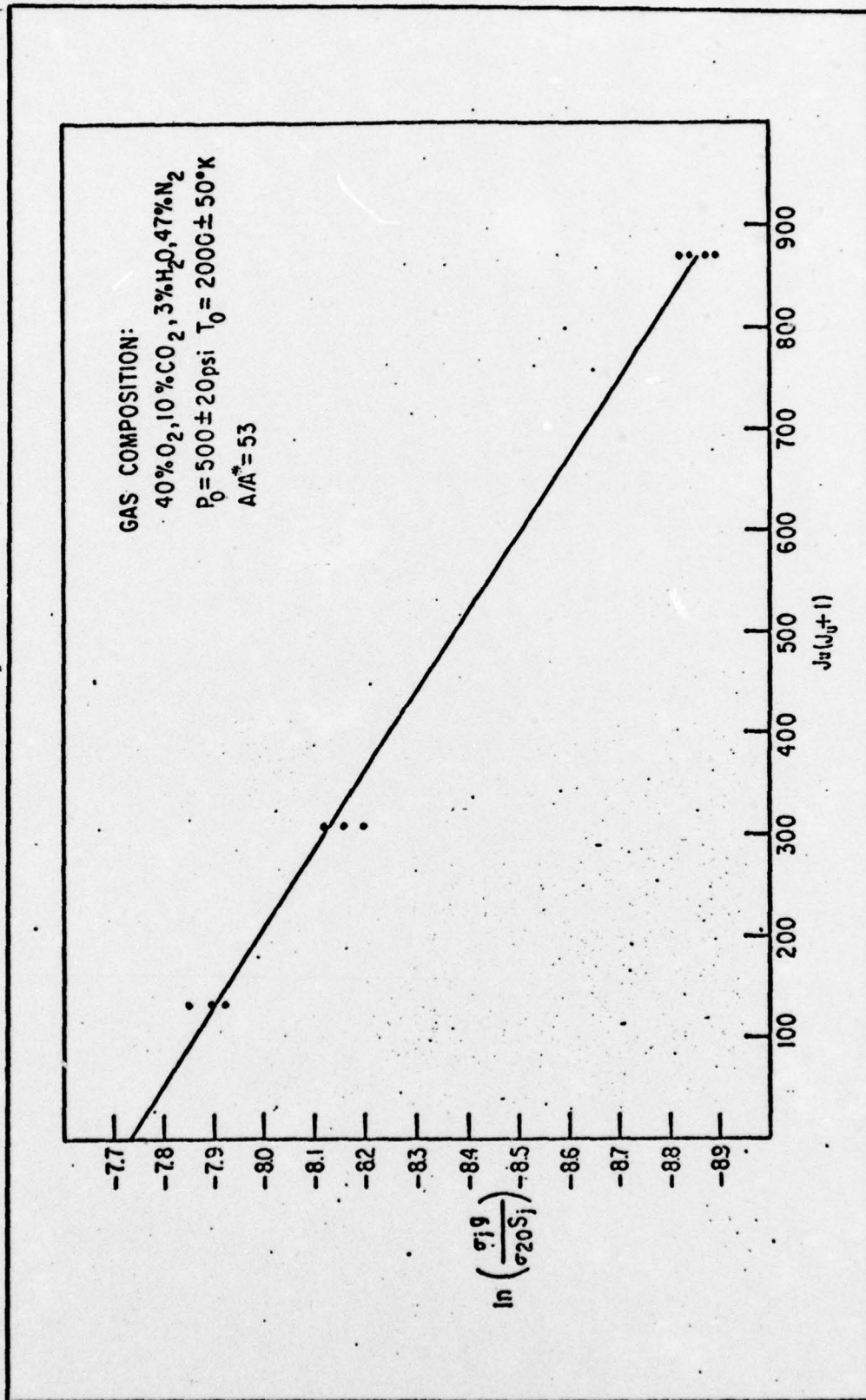


Fig. 18. J-Line Scan: 40% O₂ Case

Table X
Interpolated Results
40% Oxygen Contamination

P Line	$J_u (J_u + 1)$	$\frac{\sigma_{20} s_J}{\sigma_J}$	$\ln \left(\frac{\sigma_J g}{\sigma_{20} s_J} \right)$	$g \text{ (cm}^{-1}\text{)}$
12	132	11.3	-7.91	.0041
16	240	15.4	-8.05	.0049
18	306	17.5	-8.13	.0052
20	380	19.6	-8.23	.0052
22	462	21.7	-8.33	.0052
24	552	23.9	-8.45	.0051
30	870	30.5	-8.86	.0043

Slope = -0.001286

Intercept = -7.74

Gas Temperature = 435 °K

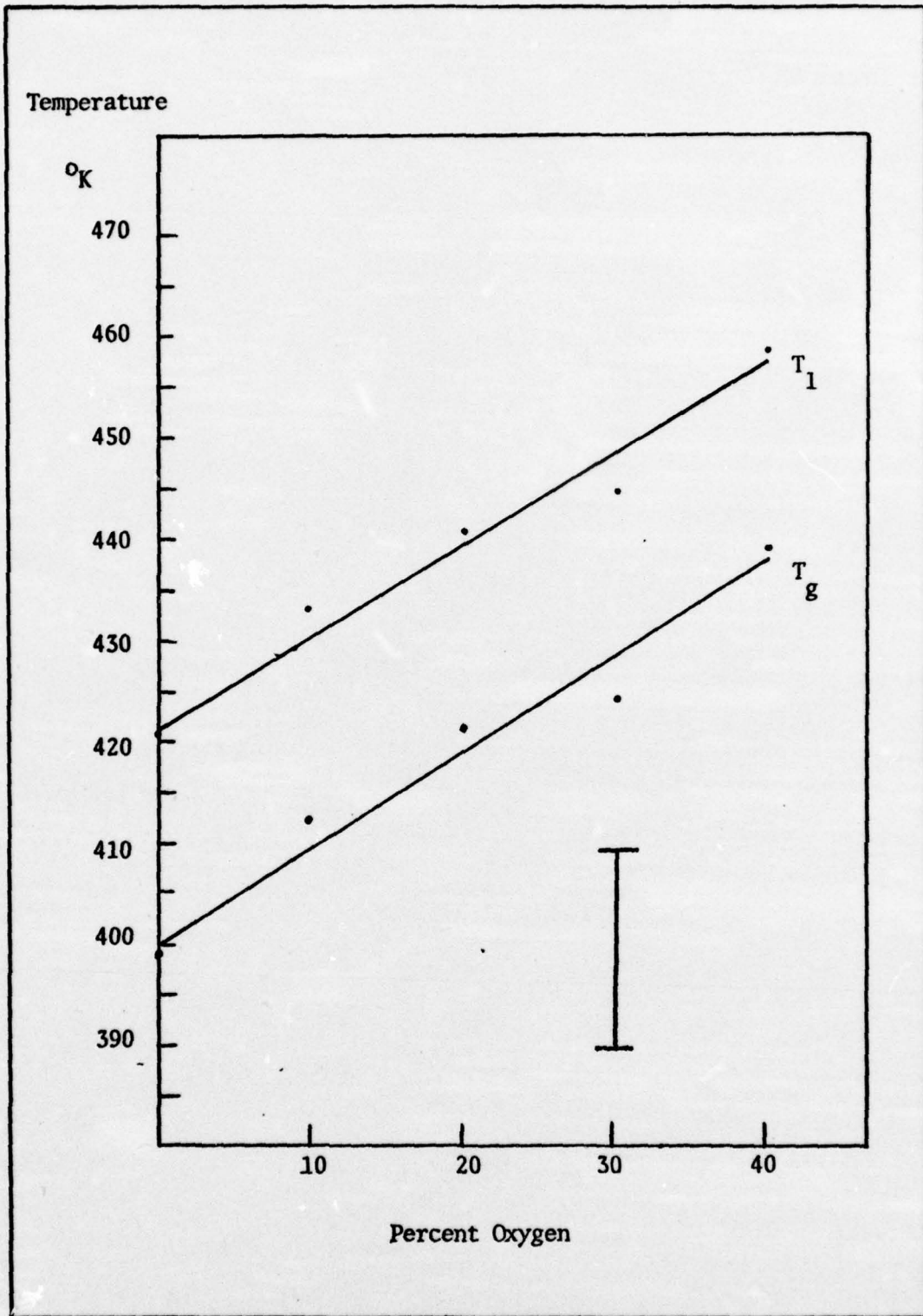


Fig.19. T, T_1 versus Percent Oxygen.

equilibrate with that of the gas is such that as the gas temperature increases, the upper laser level vibrational temperature experiences a similar increase.

Effect of O_2 On T_3 , T_N . The effect of oxygen replacement of the N_2 content of the test compositions is depicted in Figure 20. In the Figure, the oxygen excess has ranged from zero to 40% of the test mixture. The addition of O_2 in the fuel results in a marked reduction of the vibrational temperatures of both excited N_2 and the upper laser level. In other words, the introduction of 1% excess O_2 in the GDL fuel mixture was found to result in an approximate loss of 0.24% in T_3 and a 0.18% loss in T_N . This reduction in vibrational temperatures makes sense in that the temperatures reflect the total vibrational energies in the particular mode, and as such, relate the population of each mode. As more O_2 molecules replace the N_2 pumping species, T_N should decrease. Although the pumping rate of $CO_2(000)$ to $CO_2(001)$ by N_2 remains the same, a reduction in the pumping molecules results in less CO_2 molecules attaining the energy necessary to be inserted in the upper laser level. An analogous situation is that of two tanks, one small, the other large; but both equipped with the same outflow valve. When the valves are opened, the smaller tank empties prior to the larger one. In the test gas, the reservoirs are comprised of the non-contaminated gas and the excess O_2 gas. The valves on both reservoirs is the pumping rate.

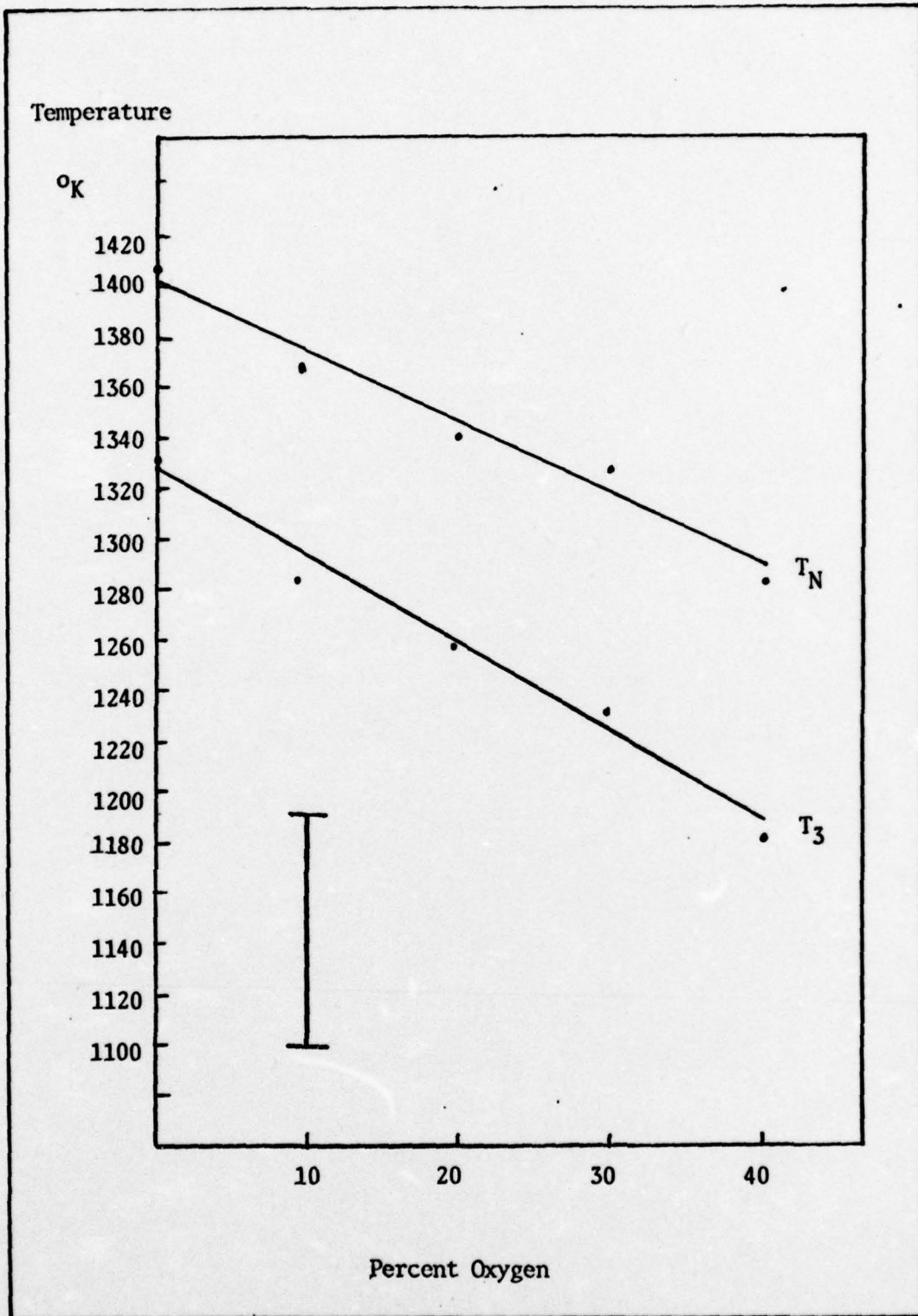


Fig. 20. T_N, T_3 versus Percent Oxygen.

Effect of O_2 on Gain. The effect of O_2 contamination on the interpolated small-signal gain coefficient is shown in Figure 21. It is seen that the interpolated peak gain suffers an approximate 0.1% degradation for each percent O_2 introduced in the test gas. The values of gain plotted in the figure are taken from the Interpolated Results Tables for each test gas. It is interesting to note that a confirmation of sorts of the J-line scan analysis can be made from the inspection of the peak gain values and the transitions on which they lie. As can be seen from the preceding tables, the rotational lines on which the peak values of g occur become less distinct as the O_2 content (and hence, the gas temperature) increases. For example, the peak gain of the 0% excess O_2 case occurs on the P(20) line only, yet the three transitions of P(18), P(20), and P(22) provide the peak gains for the 40% excess O_2 mixture. In conjunction, it should be noted that the gas temperatures of the two cases range from 399 to 435 degrees Kelvin. It is obvious that a plot of peak gain versus rotational quantum number would flatten out as the gas temperature increases. This effect is consistent with the observed phenomenon of temperature affecting the rotational population distribution of an ensemble of molecules. It can further be seen from the data that the distribution of peak gain values skews to the right (toward increasing J) for increasing gas temperatures, again consistent with known results. That is, as T increases, the peak of the rotational population distrib-

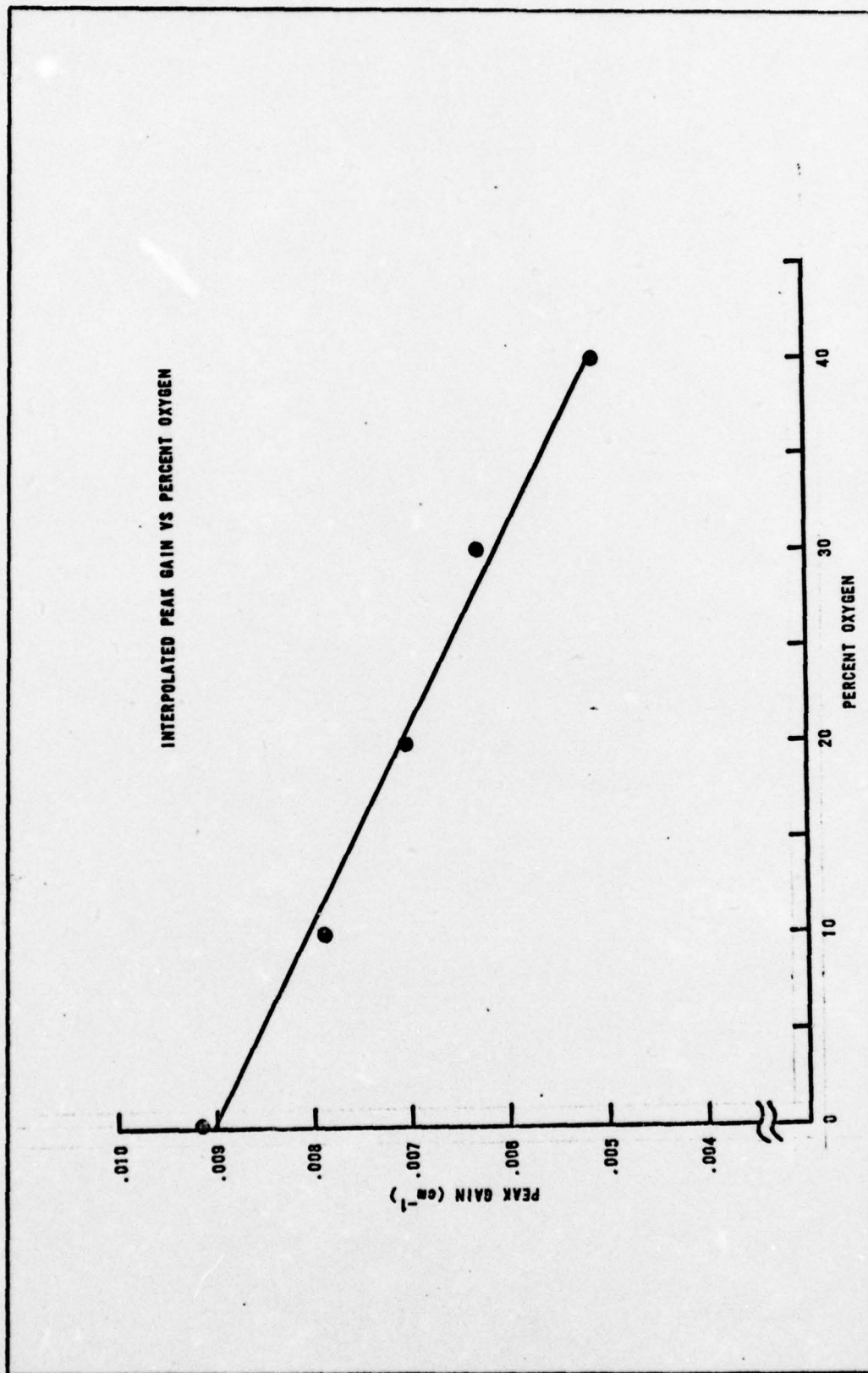


Fig. 21. Interpolated Peak Gain Versus Percent Oxygen

ution goes like:

$$J_{\max} = \sqrt{T/2\theta} - 1/2 \quad (18)$$

where θ_r is the characteristic temperature of CO_2 rotation, and is equal to $.56^\circ\text{K}$.

Because the gas temperature of the test mixture lies in the 400°K range, the rotational population distribution is not as sharply peaked as it would be if T was lower, say, at 100°K . Because of the flattening effect caused by temperature on the distribution, partial inversions are inhibited in the gases studied. The effect of such inversions have been neglected in this experiment.

Energy Available for Lasing. Figure 22 shows the effect of oxygen contamination on E_A . As seen in the Figure, E_A is plotted in units of KJ/lb and the excess O_2 ranges from 0 to 40 percent. The data produced by the AFWL theory, including degradation due to nozzle wakes in the lasing media, is shown by the upper line (through the triangles). The experimentally-derived values of E_A for each of the five gases tested are shown by the dots. The line is a least-squares fit of the data. The graph shows that the energy available for lasing decreases linearly as O_2 is introduced, replacing the nitrogen content of the mixture.

The experimental result is clearly in good agreement with theory. the slope of the curve for the theoretical degradation in E_A from O_2 is -0.218 , while that of least-

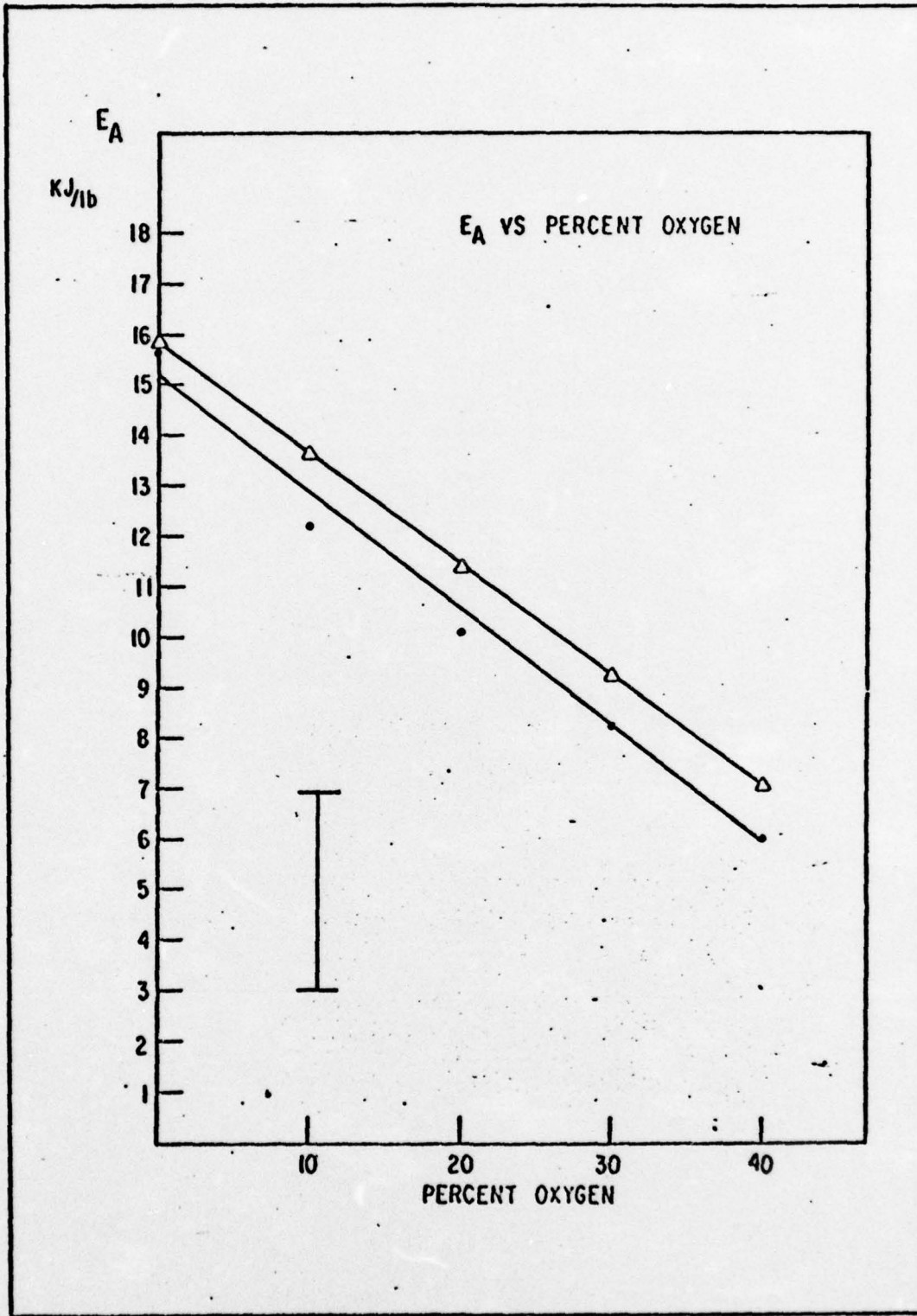


Fig.22. Energy Available Versus Percent Oxygen.

squares fit is -0.235 . The experiment shows that for the specified conditions, each percent of excess O_2 introduced in the fuel mixture results in a 1.5% loss of E_A . Theory predicts a 1.4% degradation in energy available with each percent excess O_2 .

Because of the linear relation between E_A and O_2 content, the least-squares data fit can be extrapolated to the point at which all of the N_2 is replaced by O_2 . At this point, no pumping of the CO_2 can occur and the energy available for lasing should drop to zero. Extrapolating the experimental E_A line yields an intercept on the abscissa at 65%, about 20% lower than the O_2 saturation point of 87%. Although a zero E_A point could be attained at 87% O_2 by considering the errors involved, any discrepancies in the E_A degradation can be explained by boundary layer growth in the cavity and variances in the gas compositions of each test mixture.

Summary. This experiment has shown that the performance of gas dynamic lasers does indeed suffer from the addition of excess oxygen. Oxygen contamination affects state-of-the-art GDLs, but is inherent in these devices because of their bireactant character. If a method could be found to eliminate the excessive gaseous contamination resulting from the bi-reactant mixtures fueling GDLs, energy available for lasing could be increased by about a factor of two.

It should be stated that although the linear effects of oxygen presence in the fuel of a gas dynamic laser do tend to reinforce the concept that O_2 acts merely as a diluent in the first order, the secondary effects of O_2 should not be disregarded. One such second order effect could involve an interaction between H_2O and O_2 . As seen from page 16, O_2 has its fundamental vibrational level at 1556 cm^{-1} , while H_2O exhibits a vibrational level at 1595 cm^{-1} . Because of the proximity of the energy levels, some type of energy transfer between the two species is reasonable. However, rates studies (Ref 14) indicate the importance of such an interaction to be negligible, though certainly existent.

Another effect of O_2 in the fuel of a GDL may be the deactivation of the lower laser level. It seems reasonable to expect such a depopulation since H_2O deactivates the lower laser level readily, and since O_2 exhibits a vibrational mode more closely resonant with the CO_2 (100) level than does H_2O .

Second-order effects due to the presence of oxygen in the GDL fuel should be manifested by a non-linearity in such observables as the degradation in energy available for lasing due to O_2 presence. However, though this experiment involved up to 40% O_2 in the fuel, only a linear relation for E_A with respect to O_2 content was observed. Certainly, a weak non-linearity in the data may be present which would indicate a second-order O_2 effect was involved. Thus, second order roles for O_2 cannot be disregarded, and further work must be done to ascertain their importance for the bireactant gas dynamic laser.

VI. Suggestions and Recommendations

There are several modifications that could be made to enhance the type of experiment described in this study. One of the simplest and quickest to make would be a acoustic shield surrounding the diagnostic CO₂ laser. Such a shield could easily be made from foam rubber or insulating material, and would serve to increase the stability of the probe laser. When the shock tube fires, audible sounds are produced. If the probe laser is not very stable, acoustic waves impinging upon the laser will cause variances in the laser output intensity. Such variances will be transfered to the gain trace and will be compounded by noise, resulting in errors in the measurement of gain. Another way to increase the accuracy of the gain measurement is to insure that the output from the probe laser is observed fully on the oscilloscope screen, leaving enough room for the additional gain due to the GDL. The more divisions over which the gain trace is recorded on the oscilloscope, the more accurate the measurement.

A third suggestion for future experiments is a little more complicated than the first two above. Instead of having only one beam traverse the lasing medium at an arbitrary position downstream of the nozzles, several beams could be directed into different downstream locations of the GDL. Still using only one probe laser, the beam could be directed

onto a series of beamsplitters and a mirror, and then enter the laser cavity. With this system, three or four gain measurements could be made (at various downstream locations) on each firing of the shock tube. The author investigated the possibility of using such a beamsplitting system, but found that crosstalk in the windows and beamsplitters (made of germanium) prohibited the procedure. However, salt windows should work well for this purpose. A final idea that could be used in experiments involving J-line scans is the use of two or three CO₂ diagnostic lasers. Here, one could use a small, relatively inexpensive non-tunable laser (such as a Sylvania Model 941) in conjunction with the required tunable laser. The non-tunable lasers should operate on only one rotational transition, such as the P(22) line. The tunable laser (or lasers, if two could be used) could be set to lase on a line well away from that on which the non-tunable laser is operating. Alignment of the two or three lasers should not be too difficult, and once the beams are colinear, one J-line scan could be made for each test. Also, if data on various downstream locations were desired, the multiple laser set-up could be used with the salt beamsplitter system described above. Using the multiple laser system would cut down experimental time by a factor of three. If the beamsplitter system is used, the time factor (already reduced by a factor of three) could be reduced still further by a factor equal to the number of downstream measurements desired.

Bibliography

1. Gerry, E. T., "Gasdynamic Lasers," IEEE Spectrum:7 (November 1970).
2. Newton, J. F. and Pindroh, A. L. Gain Measurements in Mixtures Containing Gaseous Contaminants. AFWL TR -74-50, AFWL, Kirtland AFB, NM (June, 1974).
3. Knoke, G. S., Wingate, F. P., and Vargas, R. E. "The Effects of Excess O₂ on Gas Dynamic Laser Performance" Laser Digest, AFWL TR-75-311 (Fall, 1975).
4. Maiman T. H. "Simulated Optical Radiation in Ruby" Nature: 187 (1960).
5. Javan, A., Bennett, W. R., Jr., and Herriot, D. R. "Population Inversion and Continuous Optical Muser Oscillation in a Gas Discharge Containing a He-Ne Mixture," Physical Review Letters, 6 (1961).
6. Christiansen, W. H. and Hertzberg, A. "Gasdynamic Lasers and Photon Machines" Private copy.
7. Basov, N. G. and Oraevskii, A. N. "Attainment of Negative Temperatures by Heating and Cooling of a System." J. of Experimental and Theoretical Physics (JETP), 44 (1963).
8. Anderson, J. D. Gasdynamic Lasers : An Introduction. Academic Press, New York (1976).
9. Knoke, G. S., private communication (July, 1976).
10. Anderson, J. D., and Harris, E. L. "Gasdynamic Laser-2 Years Later" Laser Focus: 8 (1972).
11. Taylor, R. L. and Bitterman, S. "Survey of Vibrational and Relaxational Data for Processes Important in the CO₂ - N₂ Laser System" Reviews of Modern Physics: 41 (1969).
12. Christiansen, W. H., and Tsongas, G. A. "Gain Kinetics of CO₂ Gasdynamic Laser Mixtures at High Pressure" Physics of Fluids, 14:12 (December 1971).
13. Knoke, G. S. Combusted Ludwieg Tubes for Gasdynamic Laser Research, Doctoral dissertation, available from the University of Washington (1975).
14. Center, R., and Taylor, R. L. "MSNW Rates Survey" Done for AFWL/LRL by Mathematical Sciences Northwest, Seattle, Washington (14 April 1976).

15. Knoke, G. S. Four-Temperature GDL Code. Available from AFWL/LRL Kirtland AFB, New Mexico.
16. Avizonis, P. V., Dean, D. R. and Grotbeck, R. L. "Determination of Vibrational and Translational Temperatures in Gas Dynamic Lasers" Laser Digest, AFWL-TR-73-131, (Spring 1973).
17. Tennant, R. A., et. al. Development and Application of a Low Cost Test Facility. AFWL-TR-75-268 (March 1976).
18. Knoke, G. S. J-Line Scan Analysis for CO₂ Gasdynamic Laser Gain Measurements. Flow Research Note #2103, Flow Research, Inc. (Oct 1976).
19. Wright, J. K. Shock Tubes, John Wiley and Sons, Inc. New York (1961).
20. Tennant, R. A. Unpublished Work on AFWL 4"-Shock Tube.
21. Knoke, G. S., Wingate, F. P., and Vargas, R. E. "An Experimental Study of Nozzle Wakes in Gas Dynamic Lasers" Laser Digest, AFWL TR-75-311 (Fall 1975).
22. Knoke, G. S. Computer Code for Shock Tube Conditions. Unpublished, available from AFWL/LRL.
23. Madden, M. T., Anderson, J. D. and Piper, C. H., "Equilibrium Normal Shock Properties for Vibrationally Excited CO₂ - H₂ - He Gas Mixtures" U.S. Naval Ordnance Laboratory, White Oak, Md. NOL-TR-70-103 (May 1970).
24. Herzberg, G. Infrared and Raman Spectra of Polyatomic Molecules, Van Nostrand and Co. New York (1945).
25. Mitchell, A. and Zemansky, P. Resonance Radiation and Excited Atoms, Cambridge University Press, London, 1935.
26. Herzberg, G. Spectra of Diatomic Molecules, Van Nostrand And Co. New York (1945).
27. Arié, E, et al, "Spectroscopie par Source Laser" Canadian Journal of Physics: 50,1800.
28. Langyel, B. Lasers, Wiley-Interscience, New York, 1971.

APPENDIX A

Raw Gain Data

TABLE XI

Gas Composition:

0% O₂, 10% CO₂, 87% N₂, 3% H₂O

P Line	I + ΔI (in)	I (in)	g (cm ⁻¹)
12	1.791	1.629	.0075
12	1.441	1.310	.0075
12	1.421	1.290	.0076
12	1.545	1.390	.0078
18	2.435	2.181	.0088
18	2.709	2.415	.0090
18	2.588	2.315	.0091
18	2.284	2.032	.0092
30	2.030	1.887	.0071
30	1.867	1.709	.0072
30	2.392	2.183	.0072
30	2.192	1.994	.0074

TABLE XII

Gas Composition:

10% O₂, 10% CO₂, 77% N₂, 3% H₂O

P Line	I + ΔI (in)	I (in)	g (cm ⁻¹)
12	2.305	2.130	.0062
12	2.300	2.122	.0063
12	2.590	2.390	.0063
12	2.662	2.455	.0064
20	2.395	2.175	.0076
20	2.397	2.172	.0078
20	2.399	2.173	.0078
20	2.405	2.175	.0079
30	2.275	2.108	.0060
30	1.847	1.709	.0061
30	2.245	2.075	.0062
30	2.530	2.336	.0063

TABLE XIII

Gas Composition:

20% O₂, 10% CO₂, 67% N₂, 3% H₂O

P Line	I + ΔI (in)	I (in)	g (cm ⁻¹)
12	2.502	2.334	.0054
12	2.495	2.323	.0056
12	2.435	2.268	.0056
12	2.531	2.350	.0058
20	2.548	2.279	.0071
20	2.498	2.279	.0072
20	2.521	2.290	.0076
20	2.383	2.163	.0076
30	2.276	2.125	.0054
30	2.234	2.082	.0055
30	2.290	2.124	.0059
30	2.463	2.284	.0059

TABLE XIV

Gas Composition:

30% O₂, 10% CO₂, 57% N₂, 3% H₂O

P Line	I + ΔI (in)	I (in)	g (cm ⁻¹)
12	2.118	1.985	.0051
12	2.247	2.104	.0052
12	2.393	2.237	.0053
12	2.457	2.290	.0055
20	2.500	2.300	.0066
20	2.599	2.390	.0066
20	2.515	2.310	.0067
20	2.437	2.238	.0067
30	2.482	2.330	.0050
30	2.422	2.265	.0053
30	2.489	2.322	.0055
30	2.489	2.318	.0056

TABLE XV

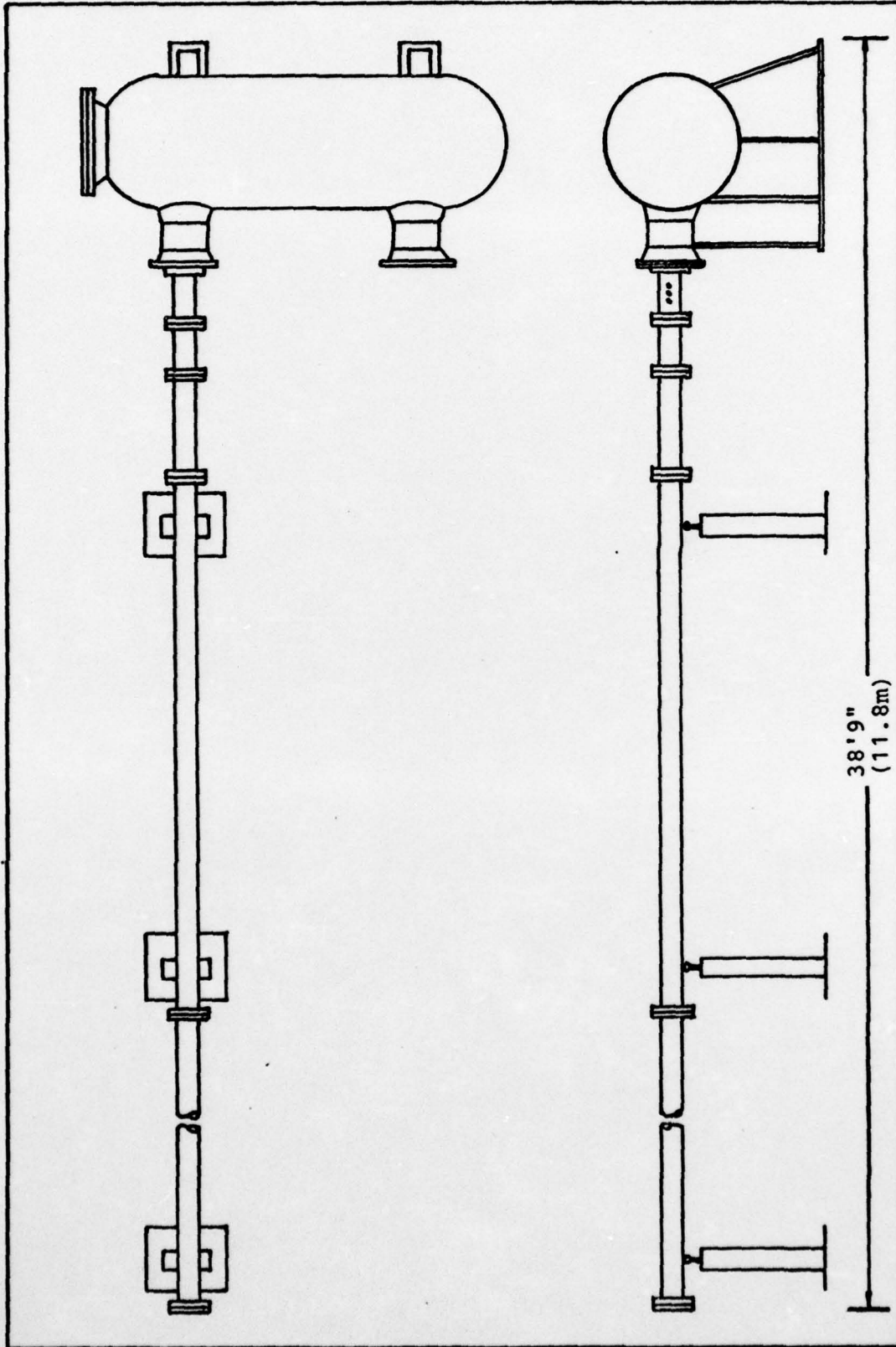
Gas Composition:

40% O₂, 10% CO₂, 47% N₂, 3% H₂O

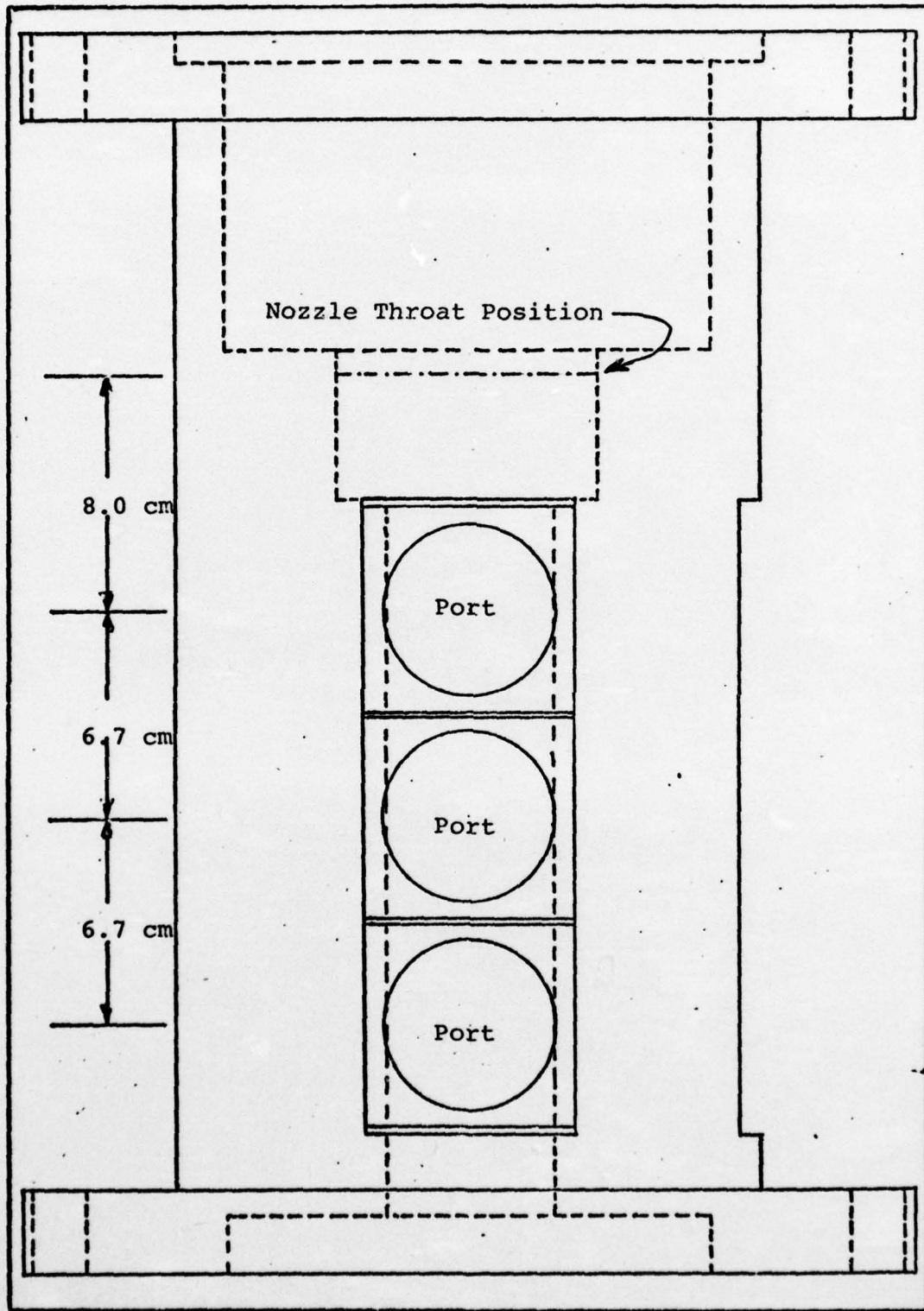
P Line	I + ΔI (in)	I (in)	g (cm ⁻¹)
12	2.445	2.320	.0041
12	2.065	1.961	.0041
12	2.321	2.199	.0042
12	2.535	2.397	.0044
18	2.082	1.962	.0047
18	2.488	2.334	.0050
18	2.256	2.112	.0052
18	2.521	2.359	.0052
30	2.300	2.182	.0042
30	2.596	2.460	.0042
30	2.355	2.228	.0044
30	2.636	2.489	.0045

APPENDIX B

Fabrication Drawings



AFWL Four-Inch Shock Tube Facility



Test Section

APPENDIX C

List of Equipment

<u>Quantity</u>	<u>Description</u>	<u>Approximate Cost</u>
1	AFWL 4" Shock Tube, with Test Section Nozzle Array Dump Tank	\$30000.00 3000.00 2000.00 250.00
1	Air Table (Modern Optics)	2760.00
	Aluminum Plates (4"X4", #1100-00)	56.00
2	Apertures	-----
1	Beam Chopper (Keithly Ins., #8403-690)	1027.00
1	Beam Steerer (Newport Res. Co., #670)	425.00
2	Beam Steerer Mirrors (NRC)	128.00
1	CO ₂ Spectrum Analyzer (Opt. Engineering)	1837.00
	Film (Polaroid)	82.00
1	Flameless Torch (Cadillac Mfg)	150.00
5	Gas Bottles (Matheson CO.)	150.00
7	Gauges, Vacuum and Pressure (Heise Co.)	2800.00
2	Gauges, Vacuum (Varian, #VT-6)	630.00
1	Germanium Beamsplitter (Co. Rad., 50/50)	25.00
2	Germanium Windows, 2" Diam.	633.00
1	Hydraulic Press (Clifton Mfg, #2B-200)	5000.00
1	Impact Wrench (Black&Decker, #6821)	85.00
1	Infrared Detector (PIRE, #HCT-150)	900.00
1	Interference Filter	15.00
2	Lab Jacks (NRC)	900.00
1	Laser System, CO ₂ (Coh. Rad. #42), with: Cooling Unit Gas Supply Power Supply Shutter Control (Model 407)	35000.00

APPENDIX C (Cont)

1	Laser System, CO ₂ (Sylvania 950 A/B)	\$15000.00
1	Oscilloscope, Tektronix (#7904A), with: Camera Attachment 7A22 Diff. Amps. 7B71 Time Base 7M13 Readout Unit	8000.00
2	Piezoelectric Pressure Transducers (Kistler #202A2)	1000.00
1	Power Meter (Coh. Rad # 201)	1065.00
2	Pressure Amps., (Kiestler, #583C)	1340.00
1	Sandblasted Aluminum Plate	--
1	Timer (Eldorado, #255)	425.00
1	Vacuum Pump (Welch #1398)	1123.00
1	Vacuum Pump (Welch #1397)	840.00
1	Vacuum Pump (Welch Special Model)	284.00
		<hr/>
		\$116930.00

AD-A034 900

AIR FORCE INST OF TECH WRIGHT-PATTERSON AFB OHIO SCH--ETC F/6 20/5
EFFECTS OF OXYGEN CONTAMINAT CN ON GAS DYNAMIC LASER PERFORMANC--ETC(U)
DEC 76 J B WATTERSON

UNCLASSIFIED

GEP/PH/76D-12

NL

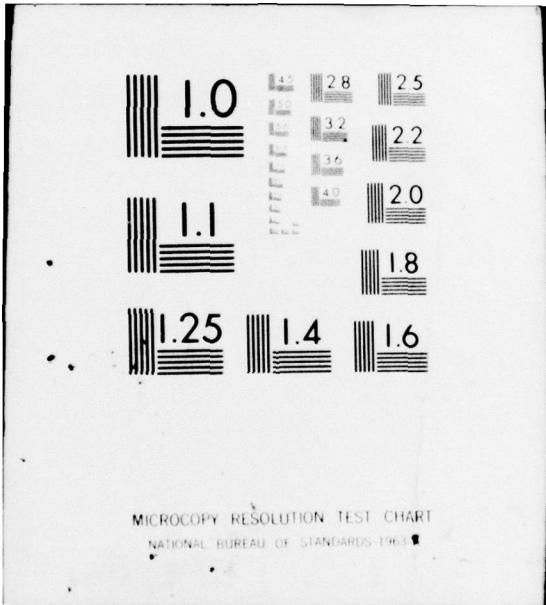
2 of 2

AD
A034900



END

DATE
FILMED
2-77



APPENDIX D

Data on Instrumentation

1. HgCdTe IR Detector

Manufacturer: Princeton Infrared Equipment, Inc (#HCT-50)

Description:

Length: 0.51 mm Width: 0.51mm Active Area: $2.6 \times 10^{-3} \text{ cm}^2$

Peak Wavelength: 13.5 Cut-off Wavelength: 14.5

Operating Temperature: 77°K

Background Temperature: 300°K

Bias Current (ma)	Noise (nv/Hz)	Reponsivity at 12 (V/W)	D* (12 ,10KHz,1)
25.4	1.98	166	4.27
35.2	2.43	206	4.32
49.0	2.97	264	4.53

2. Quartz Piezoelectric Pressure Transducers

Manufacturer: Kistler Instrument Co. (Model 202A2)

Max Pressure: 2000 psi Sensitivity: 10 mV/psi

Resolution: .02 psi Thermal Sensitivity Shift: $0.04 \%/^\circ\text{F}$

Rise Time: (10% to 90%) $1 \times 10^{-6} \text{ s}$

APPENDIX E

Area Ratio Data

1. Nozzle Exit Plane

$$\begin{aligned}
 A_{1-8} &= 1.5118 \text{ in}^2 \\
 A_2 &= 1.4825 \\
 A_3 &= 1.4827 \\
 A_4 &= 1.4624 \\
 A_5 &= 1.4460 \\
 A_6 &= 1.4450 \\
 A_7 &= 1.4800
 \end{aligned}$$

2. Nozzle Entrance Plane

$$\begin{aligned}
 A_{1-8}^* &= 0.02359 \text{ in}^2 \\
 A_2^* &= 0.03008 \\
 A_3^* &= 0.03156 \\
 A_4^* &= 0.03295 \\
 A_5^* &= 0.02509 \\
 A_6^* &= 0.02864 \\
 A_7^* &= 0.02429
 \end{aligned}$$

3. Nozzle Element Area Ratios

$$\begin{aligned}
 A/A_{1-8}^* &= 64.1 \\
 A/A_2^* &= 49.3 \\
 A/A_3^* &= 47.0 \\
 A/A_4^* &= 44.4 \\
 A/A_5^* &= 57.6 \\
 A/A_6^* &= 50.5 \\
 A/A_7^* &= 59.7
 \end{aligned}$$

$$(A/A^*)_{\text{ave}} = 53$$

$$h^* = 0.034 \text{ cm}$$

APPENDIX F

Derivation of Small-Signal Gain Coefficient

The formula used to define the small-signal gain coefficient, g , is derived from the absorption line equation given in Reference 25:

$$\int \alpha_\nu d\nu = \frac{\lambda_0^2}{8\pi} \frac{g_2}{g_1} \frac{N_1}{\tau_{21}} \left(1 - \frac{g_1 N_2}{g_2 N_1}\right) \quad (\text{Ref 25:95}) \quad \text{F.1}$$

where α_ν = the absorption coefficient of the media, and λ_0 = the wavelength at the center of the line. The g_i term correspond to the statistical weight of the i -th level. A line shape factor, ϕ , can be associated with the absorption coefficient such that

$$\alpha_\nu = \int \alpha_\nu d\nu (\phi(\nu - \nu_0)) \quad (\text{Ref 8}) \quad \text{F.2}$$

Since the small-signal gain can be written is the negative absorption coefficient, Eq A.1 becomes the following upon substitution:

$$g = \frac{\lambda_0}{8\pi} \frac{g_2}{g_1} \frac{1}{\tau_{21}} \phi \left(-\frac{g_1}{g_2} N_2 - N_1\right) \quad \text{F.3}$$

Now the $1/\tau_{21}$ term is the Einstein "A" Coefficient; that is,

$$1/\tau_{21} = A_{21} = \frac{64 \pi^4}{3hc^3} \nu^3 g_1 |R_{\ell m}(m)|^2 \quad (\text{Ref 26}) \quad \text{F.4}$$

where $|R_{\ell m}(m)|^2$ is the vibrational transition matrix element. According to Reference 27, the rotational dependence (characterized by m) can be separated from the matrix

element so that:

$$|R_{\ell m}(m)|^2 = |R_{\ell m}|^2 F(m) \quad \text{F.5}$$

where $m = -J = -(J_u+1)$ for P-branch CO_2 transitions.

Further,

$$F(m) = 1 - 0.0009m - 0.00006m^2 \quad \text{F.6}$$

for the (001) to (100) transition of CO_2 (Ref 27).

Substituting Eqs A.4 and A.5 into the gain equation (Eq A.3) gives:

$$g = \frac{8\pi^3}{3hc\lambda_{21}} |R_{\ell m}|^2 F(m) \phi g_2 (N_2/g_2 - N_1/g_1) \quad \text{F.7}$$

But Reference 28 shows that for CO_2 (with N_c molecules in the ground state), the number of molecules in the upper level, N_2 , is

$$N_2 = \frac{N_c}{Q_R Q_V} \exp\left[-\frac{\theta_3}{T_3} - J_u(J_u+1) \frac{\theta_R}{T}\right] \quad \text{F.8}$$

and similarly for the number of CO_2 molecules in the lower laser level,

$$N_1 = \frac{N_c}{Q_R Q_V} \exp\left[-\frac{\theta_\ell}{T_\ell} - J_\ell(J_\ell+1) \frac{\theta_R}{T}\right] \quad \text{F.9}$$

Definitions of the terms in the above two equations are given in the List of Symbols, page viii, of this text.

The J-line scan method of Knoke (Ref 18) makes the approximation

that the rotational dependence of the vibration-rotation transition matrix element is equal to the rotational degeneracy of the upper laser level. Thus, $|m| = g_2$. By substituting the above as well as Eqs A.8 and A.9 into the gain equation, Eq A.7, The small-signal gain becomes:

$$g = \frac{8\pi^3}{3hc\lambda_{21}^2} |R_{\ell m}|^2 F(m) \frac{|m| N_c}{Q_r Q_v} \phi [e^{-\theta_3/T_3} - J_u(J_u+1)\theta_r/T - e^{-\theta_\ell/T_\ell} - J_\ell(J_\ell+1)\theta_r/T]$$

E.10

The expression for the small-signal gain above is used (in the text) to derive the gain at line center for collision-broadened lines.

APPENDIX G

Derivation of Energy Available for Lasing

An expression for the energy available for lasing, E_A , can be found by assuming that all of the vibrational energy in the nitrogen molecules is transferred to the the CO_2 molecules in the (001) mode. However, because lasing ceases when the gain goes to zero and the population inversion disappears, some residual vibrational energy remains in the N_2 and CO_2 mode 3 which must be taken into account (Ref 18:12). Because the energy available for lasing is determined by the vibrational energy in the CO_2 and N_2 molecules, E_A can be written as

$$E_A = \sum_i N_i \epsilon_i = N_i k \theta_i \quad \text{G.1}$$

where N_i = number of a particular species possessing a characteristic temperature θ_i ($= h\nu_i/k$). Considering, for example, only the nitrogen molecules,

$$N_i = [N e^{-\theta_i/T}] / Q_V \quad \text{G.2}$$

where Q_V is the vibrational partition function. That is,

$$Q_V = \sum_j e^{-j h \nu / k T} \quad \text{G.3}$$

Now Q_V can be expressed as a simple geometric series:

$$\frac{1}{1-x} = 1+x+x^2+\dots = \sum_j x^j \quad \text{G.4}$$

with $x = e^{-h\nu/kT}$.

Thus, the vibrational partition function is

$$Q_v = \frac{1}{1 - e^{-\theta/T}} \quad \text{G.5}$$

Substituting this result into Eq G.2 yields

$$N_i = [N e^{-h\nu_i/kT}] [1 - e^{-\theta/T}] \quad \text{G.6}$$

Substitution of Eq G.6 into G.1 gives

$$E_A = N [1 - e^{-\theta/T}] \sum_i \epsilon_i e^{-\epsilon_i/kT} \quad \text{G.7}$$

Or,

$$E_A = N \sum_i \epsilon_i e^{-\epsilon_i/kT} [1 - e^{-\theta/T}] \{1 + 2e^{-\epsilon/kT} + 3e^{-2\epsilon/kT} + \dots\} \quad \text{G.8}$$

$$= N \sum_i \epsilon_i e^{-\epsilon_i/kT} [1 - e^{-\theta/T}] \left[\frac{1}{(1 - e^{-\epsilon/kT})^2} \right]$$

$$= N \sum_i \epsilon_i e^{-\theta/T} [1 - e^{-\theta/T}] [1 - e^{-\theta/T}]^{-2}$$

$$E_A = N \epsilon [e^{\theta/T} - 1]^{-1} \quad \text{G.9}$$

Similar expressions can be obtained for the CO_2 molecules.

The energy available for lasing from the entire gas mixture is a combination of these terms; positive contributions to E_A come from the vibrational energy in the CO_2 mode 3 and in the N_2 molecules. The residual energy is a negative contribution. Defining the energy term,

$$\epsilon = (R_u/M) [\theta_3 - \theta_2] \quad \text{G.10}$$

where R_u is the universal gas constant [8.314 J/(mole-°K)], M is the molecular weight of the gas [gram/mole] and θ_3 , θ_l are the vibrational temperatures of the upper and lower laser level [°K], respectively. Note that the units of the energy term are J/gram. This energy term must then be multiplied by the species contributions discussed earlier. The result is:

$$E_A = R_u M^{-1} (\theta_3 - \theta_l) \left[\psi_C / (e^{\theta_3/T_3} - 1) + \psi_N / (e^{\theta_N/T_N} - 1) - (\psi_C + \psi_N) / (e^{\theta_l/T_l} - 1) \right] \quad G.11$$

Converting the value of E_A to units of kilojoules per pound,

$$E_A = 3.77 M^{-1} (\theta_3 - \theta_l) \left[\psi_C / (e^{\theta_3/T_3} - 1) + \psi_N / (e^{\theta_N/T_N} - 1) - (\psi_C + \psi_N) / (e^{\theta_l/T_l} - 1) \right] \quad G.12$$

VITA

John Brett Watterson was born on September 10, 1949 in New York, New York. He graduated from high school in 1967 from Littleton High School, Colorado. In the same year, he entered the Virginia Military Institute. There he learned for himself what Pascal knew centuries before: "The heart has reasons reason knows nothing of". Upon graduation from VMI in 1971, he received the degree of B. Sc. in Physics and a commission in the United States Air Force. Following graduation and prior to entering in the service, he traveled through Western Europe as well as studied Shakespeare and Modern Drama at Oxford University in England. Called to active duty in October of 1971, he attended the Air Intelligence Training Center, Lowry AFB, Colorado for five months. He then served as an Air Intelligence at Korat Royal Thai Air Force Base, Thailand until April, 1973. He was next assigned to the Foreign Technology Division as a Current Intelligence Analyst until June of 1975, when he was fortunate enough to enter the Air Force Institute of Technology.

UNCLASSIFIED

SECURITY CLASSIFICATION OF THIS PAGE (When Data Entered)

REPORT DOCUMENTATION PAGE		READ INSTRUCTIONS BEFORE COMPLETING FORM
1. REPORT NUMBER GEP/PH/76D-12	2. GOVT ACCESSION NO.	3. RECIPIENT'S CATALOG NUMBER
4. TITLE (and Subtitle) EFFECTS OF OXYGEN CONTAMINATION IN GAS DYNAMIC LASERS		5. TYPE OF REPORT & PERIOD COVERED MS Thesis
		6. PERFORMING ORG. REPORT NUMBER
7. AUTHOR(s) John B. Watterson, Capt USAF		8. CONTRACT OR GRANT NUMBER(s)
9. PERFORMING ORGANIZATION NAME AND ADDRESS Air Force Institute of Technology (AFIT-EN) Wright-Patterson AFB, Ohio 45433		10. PROGRAM ELEMENT, PROJECT, TASK AREA & WORK UNIT NUMBERS
11. CONTROLLING OFFICE NAME AND ADDRESS Air Force Weapons Laboratory (ARTO/LRL) Kirtland AFB, N.M. 87117		12. REPORT DATE December, 1976
		13. NUMBER OF PAGES 92
14. MONITORING AGENCY NAME & ADDRESS (if different from Controlling Office)		15. SECURITY CLASS. (of this report) Unclassified
		15a. DECLASSIFICATION/DOWNGRADING SCHEDULE
16. DISTRIBUTION STATEMENT (of this Report) Approved for public release; distribution unlimited		
17. DISTRIBUTION STATEMENT (of the abstract entered in Block 20, if different from Report)		
18. SUPPLEMENTARY NOTES Approved for public release; IAW AFR 190-17 JERRAL F. GUESS, Captain, USAF Director of Information		
19. KEY WORDS (Continue on reverse side if necessary and identify by block number) Gas Dynamic Laser Bireactant GDL Shock Tube-Driven GDL J-Line Scan GDL		
20. ABSTRACT (Continue on reverse side if necessary and identify by block number) The effects of oxygen in the fuel of a shock-tube driven gas dynamic laser was observed with the four-inch shock tube of the Air Force Weapons Laboratory, Kirtland AFB, New Mexico. Five test gases comprised of ten percent CO ₂ , three percent H ₂ O, and varying amounts of N ₂ and O ₂ were studied. Nominal stagnation conditions were 2000 K and 500 psia. The small-signal gain coefficient was measured on three different rotational transitions for each test gas, permitting a J-line scan to be performed. → next page		

UNCLASSIFIED

SECURITY CLASSIFICATION OF THIS PAGE(When Data Entered)

→ The gas temperature, vibrational temperature of the upper laser level, and energy available for lasing were calculated using the J-line scan method. It was found that the small-signal gain coefficient, the vibrational temperature of the upper laser level, and the energy available for lasing all decreased linearly as the oxygen concentration in the gas dynamic laser fuel increased. Specifically, an increase in the oxygen content of 1% resulted in a decrease of the gain coefficient by roughly 1.5%. Such a decrease is in agreement with previous work performed at the Air Force Weapons Laboratory. ↗

UNCLASSIFIED

SECURITY CLASSIFICATION OF THIS PAGE(When Data Entered)